

A new soil-based approach for empirical monitoring of enhanced rock weathering rates

Tom Reershemius^{1*} and Mike E. Kelland^{2*}, Isabelle R. Davis^{1,3}, Rocco D'Ascanio¹, Boriana Kalderon Asael¹, Dan Asael¹, Dimitar E. Epihov², David J. Beerling², Christopher T. Reinhard⁴, Noah J. Planavsky¹

¹Department of Earth and Planetary Sciences, Yale University, New Haven, CT, USA

²Leverhulme Centre for Climate Change Mitigation, School of Biosciences, University of Sheffield, Sheffield, UK

³School of Ocean and Earth Science, University of Southampton Waterfront Campus, Southampton, UK

⁴School of Earth and Atmospheric Sciences, Georgia Institute of Technology, GA, USA

*corresponding and equal contribution authors: tom.reershemius@yale.edu, mekelland1@sheffield.ac.uk

Significance statement: Greenhouse gas management through carbon dioxide removal (CDR) could be implemented to augment mitigation of CO₂ emissions, increasing the chances of meeting international climate goals. Enhanced rock weathering (ERW) is a form of CDR that has the potential to permanently remove billions of tons of carbon dioxide from the atmosphere. However, effective implementation of this approach must entail robust monitoring, reporting and verification (MRV). We describe and empirically validate a geochemical mass-balance approach for tracking rates of carbon capture through ERW that has the potential to be tractable at scale.

Abstract: Enhanced rock weathering (ERW) has been touted as a scalable and cost-effective potential carbon dioxide removal (CDR) strategy with significant environmental and agronomic co-benefits. However, a major barrier to implementation of ERW at scale is a robust monitoring, reporting, and verification (MRV) framework that can accurately, precisely, and cost-effectively measure the amount of carbon dioxide being removed by ERW in the field. Here we outline a new method based on mass balance in which metal analysis in soil samples is used to accurately track the extent of *in-situ* alkaline mineral weathering. We show that signal-to-noise issues can be overcome by using isotope-dilution mass spectrometry to reduce analytical error. We provide an example of implementation of this method in a controlled mesocosm experiment. Using this approach, we calculate an average initial CDR value of 1.06 ± 0.50 tCO₂eq ha⁻¹ from our experiments after 235 days, within error of an independent estimate calculated using a conventional reaction product-based approach. Our method provides a robust time-integrated estimate of CDR potential that avoids the need to trace and measure soluble ERW reaction products and is designed to integrate seamlessly with existing agronomic practices. We suggest that these features render the approach less likely to encounter prohibitive barriers to scale than alternative techniques, providing the potential to confidently track and validate carbon removal through ERW.

1 Introduction

Avoiding 1.5°C or even 2°C of global warming by 2100 will require countries to meet their current nationally determined contributions (NDCs) toward decarbonization through short-term policy implementation, and to continue setting increasingly stringent year-on-year mitigation targets (1, 2). Despite progress in setting NDCs in recent years, the median gap between mitigated greenhouse gas (GHG) emissions after implementation of all conditional NDCs and emissions scenarios that prevent 2°C of warming will be 12 gigatonnes (10⁹ tonnes) of CO₂ equivalent emissions (GtCO₂eq) by 2030; the gap from current policies is far greater still (3). In the absence of feasible pathways to achieve net-zero carbon emissions, large-scale carbon dioxide removal (CDR) will very likely be a necessary additional measure for augmenting decarbonization in efforts to achieve net-zero carbon emissions in the coming century (e.g., 4, 5).

Enhanced rock weathering (ERW) is a potentially promising CDR technique whereby naturally occurring mineral weathering reactions that consume atmospheric CO₂ are accelerated, typically by applying crushed silicate rocks with a high reactive surface area to agricultural and forest soils (e.g., 6-20). Potential advantages and co-benefits of ERW include: a low technological barrier to implementation at scale (8, 13); long-term (>1000 year) storage of carbon compared to organic reservoirs (21-27); supply of key nutrients for crop growth (13, 28-33); and deacidification of soils, where ERW feedstocks such as basalt can fill the same role as agricultural lime (currently a net source of CO₂ to the atmosphere; 34-42). Several recent advances make upscaling of ERW more likely: mechanistic modelling of weathering reactions in agricultural soils (e.g., 11, 14, 43); modelling how hydrology affects ERW (e.g., 44); laboratory and mesocosm experiments tracking uptake of nutrients by plants and feedstock dissolution rates (e.g., 30, 32, 42, 45-51); and field experiments implementing ERW at scale (e.g., 52-54).

Despite these advances, ERW currently lacks a robust framework for monitoring, reporting, and verification (MRV) of CDR rates. This is currently a major barrier to widespread implementation on a voluntary and/or compliance market, as there are still major uncertainties pertaining to ERW, primarily in weathering rates in field settings with varying hydroclimatic conditions (e.g., 55). At the same time—while they can be useful in the aggregate for making testable predictions (e.g., 14, 19, 43)—it is not yet clear whether the current generation of reaction-transport models for simulating ERW is capable of accurately predicting deployment-level rates of carbon removal in a way that keeps key stakeholders in a healthy CDR landscape can be confident. Bringing ERW to scale will thus require an empirical MRV framework that can report site- and time-specific rates of feedstock weathering while being cost-effective and minimally invasive (e.g., 56, 57).

Here we introduce a novel soil-based mass balance approach for quantitatively tracking enhanced rock weathering in soils. Our approach measures the difference in concentration of ERW feedstock *in-situ* before and after weathering. This builds on a technique that is widely used to gauge the extent and style of weathering in natural systems (e.g., 58-70). We compare the concentrations of metal cations (Ca²⁺, Mg²⁺, Na⁺) in the solid phase of soils before and after feedstock deployment. We do this by estimating changes in the total amount of these metal cations (CAT) in a specific soil sample relative to the concentration of an immobile tracer, in this case titanium (Ti; **Figure 1**) – a method referred to here as TiCAT. As a first step towards robust validation, we compare estimates of the extent of *in-situ* basalt feedstock dissolution from TiCAT to rates determined

independently from detailed pool and flux tracking in a mesocosm experiment (see 32). We then discuss the practical advantages of this approach for at-scale deployment of CDR through ERW, and the steps require to move from an empirical estimate of feedstock dissolution rates to robust error-bound estimates of carbon removal.

2 Theory

2.1 Solid sample mass balance approach to quantifying mineral weathering

TiCAT is a mass balance approach for estimating the time-integrated amount of basalt feedstock in a soil sample that has undergone weathering. This method builds from common approaches for estimating the extent of soil weathering in natural systems (e.g., 58-70). These approaches define a mass transfer function for a mobile element j , τ_j , such that:

$$\tau_{j,w} = \frac{m_{j,flux}}{m_{j,p}} = \left(\frac{c_{j,w}}{c_{i,w}} \right) / \left(\frac{c_{j,p}}{c_{i,p}} \right) - 1$$

where m is mass; c is concentration; p is unweathered parent material; w is weathered material (and thus *flux* refers to mass lost from parent material during weathering); and i is a reference immobile element (59).

Within the TiCAT framework, this involves calculating changes in the concentrations of major cations (j) in soils that have been amended with basalt. To define an unweathered parent material p , we first compare soil samples after basalt amendment with soil samples representative of a pre-amendment baseline, as well as samples of the basalt feedstock. This can be most readily be visualized as simple two-component mixing between a soil (c_{soil}) and a basalt (c_{basalt}) endmember (**Figure 1a**). The difference in concentration of an immobile trace element i (e.g., Ti) between a post-application sample and the pre-application soil baseline ($Ti_{end} - Ti_{soil} = Ti_{add}$) is used to calculate the amount of basalt that has been added to the original soil for the specific sample analyzed.

Titanium is commonly used as a reference element for immobility during weathering processes due to its low solubility, the chemical stability of minerals within which it is abundant (e.g., rutile, titanite), and the tendency of those minerals to form insoluble secondary minerals during weathering (see 61, 71-75). A similar approach could be used with other largely immobile elements such as zirconium (Zr), thorium (Th), niobium (Nb) and tantalum (Ta) (see 61, 75-79). Aluminium (Al) and Rare Earth Elements are, in many cases, also immobile (e.g., 78, 80-84). Here we focus on Ti due to its higher abundance in mafic minerals that constitute the best ERW feedstocks and the less onerous process of dissolving Ti for laboratory analysis compared to Zr (85). It is important to note, however, that the assumption that Ti acts as an immobile element during weathering must be treated with some caution, as in rare cases Ti, Zr and Th — similar to Al and REEs — act as semi-mobile elements during weathering. However, these predominantly occur during extended periods of weathering in which the soil becomes extensively depleted in cations — in strong contrast to the conditions in this experiment or those expected to prevail during enhanced weathering deployments (75, 79, 86-90).

Using the relative abundance of Ti and mobile major cations (CAT) in the original basalt feedstock, we can calculate the corresponding amount of mobile major cations (CAT_{add}) from the basalt feedstock present in the soil-basalt mixture at the point of basalt application (**Figure 1b**). For a generic cation, CAT:

$$Ti_{add} * \frac{CAT_{basalt} - CAT_{soil}}{Ti_{basalt} - Ti_{soil}} + y = CAT_{add} \quad ,$$

where y is the CAT intercept of the mixing line. Subtracting from this the amount of cation CAT in the post-application sample (CAT_{end} – see **Figure 1c**) and adding the soil baseline (CAT_{soil}), we calculate the difference in the amount of the mobile cation, ΔCAT , between the expected amount from addition of basalt, and the observed amount in the soil/basalt mixture after weathering (**Figure 1d**):

$$CAT_{add} + CAT_{soil} - CAT_{end} = \Delta CAT \quad .$$

ΔCAT therefore represents the amount of basalt dissolved (i.e., lost from the solid phase) between the point of basalt application and the post-application sampling date. We can also express the amount of basalt dissolution as $f_{dissolution}$, where:

$$f_{dissolution} = \frac{\Delta CAT}{CAT_{add}} \quad .$$

Or, in the canonical mass transfer framework: $c_{j,w} = CAT_{end}$; $c_{i,w} = Ti_{end}$; $c_{j,p} = CAT_{add} + CAT_{soil}$; $c_{i,p} = Ti_{add} + Ti_{soil}$; thus:

$$f_{dissolution} = -\tau_{j,w} \left(\frac{CAT_{add}}{CAT_{soil}} + 1 \right) \quad .$$

Note that here, $f_{dissolution}$ of basalt specifically pertains to each cation of interest. For the purposes of estimating CDR the major cations in basalt are Na^+ , K^+ , Ca^{2+} , and Mg^{2+} . We disregard K^+ here, both because it is a constituent of the NPK fertilizer added to some of our mesocosm experiments and because it represents only a minor portion of the overall cation load. An extension of this scheme is to define an additional endmember representing the dissolved fraction of basalt ($C_{dissolved}$), which comprises the Ti concentration of the basalt endmember, but has lost all mobile elements from the solid phase (i.e. $CAT_{dissolved} = 0$). This allows us to solve iteratively for all mixtures that satisfy the relationship $c_{sample} = c_{soil} + c_{basalt} + C_{dissolved}$, and thus identify the most likely $f_{dissolution}$ that has occurred to give a specific combined Ti and CAT signal.

2.2 Analytical requirements

Limiting analytical error is a critical aspect of the TiCAT approach and will likely be critical for any approach meant to track CDR from the solid phase given the signal-noise associated with adding feedstock to a large mass of background soil. For technically and commercially feasible feedstock application rates (likely $<5-50 \text{ t ha}^{-1}$, see 13), analytical error can result in overlap between error-bounded values for cation concentration of soil-feedstock mixtures before and after dissolution has occurred. For instance, at 5% analytical error a 75% loss of major cations from the basalt portion of a soil-feedstock mixture is resolvable only at an application rate of $\sim 40 \text{ t ha}^{-1}$, assuming the mixture is homogenized to a depth of 10cm (a common mixing regime for managed row crop systems). At 1% analytical error the same amount of cation loss is resolvable at $\sim 5 \text{ t ha}^{-1}$ (**Figure 2**). When accounting for a range of plausible dissolution and application rates analytical error must generally be limited to $\sim 1\%$ for our mass balance method to be accurate and widely

applicable, a standard that is more stringent than that currently achievable by most commercial inorganic mass spectrometry analyses (e.g., 91, 92).

We obtained the requisite analytical precision for the TiCAT method using isotope dilution inductively coupled plasma mass spectrometry (ID-ICP-MS). Isotope dilution is an analytical method whereby the concentration of an element in a sample can be measured from the known concentration of an element in a spike solution, and the ratios of two isotopes of the same element in the natural sample and the spike respectively (e.g., 93; see also 94, 95; and see *Supplemental Information Section 1.7*). Our results show that our isotope dilution technique allows for a level of measurement accuracy and precision on quadrupole ICP-MS instruments that would otherwise only be achievable with a magnetic sector (**Figure 3**; see also 96). Given its much lower cost and far greater availability, the ability to leverage quadrupole ICP-MS for fast analyses may be a critical factor in making this MRV technique economically viable at scale.

3 Method

As an initial test of the TiCAT method we employed mesocosm experiments, which allow us to independently estimate CDR by measuring the concentration of reaction products in exchange/solute pools (see 28, 30, 32, 45-49, 51, 54). Each mesocosm contained a single specimen of the cereal crop *Sorghum bicolor* (see 32) with two different fertilizer treatments (nitrogen-phosphorus-potassium, NPK, or manure), to which a basalt feedstock was added equivalent to an application rate of 5 kg m⁻² (50 t ha⁻¹; for a detailed description of mesocosm design and construction, substrate and feedstock preparation and characterization, plant varieties and growth conditions, and irrigation regime see *Supplemental Information*). After 235 days, samples were taken from relevant chemical pools — the soil exchangeable fraction, the solid phase with the exchangeable fraction removed, the leachate solution, and the plant material. We obtain an initial CDR estimate based on the solid phase by calculating $A_{CATdiss}$ (the total mass of cation in feedstock applied over a given area that was dissolved; see *Supplemental Information Section 1.10*) for Na⁺, Ca²⁺, and Mg²⁺ for each of the mesocosms in this study as described above. This can then be compared to an initial CDR estimate obtained by quantifying the excess of elemental budgets of Na⁺, Ca²⁺, and Mg²⁺ in all dissolved or non-mineral-bound pools (leachate + soil exchangeable sites + plant material) in basalt-treated mesocosms relative to an average of mesocosms where no basalt was applied.

4 Results and Discussion

Our results show a strong agreement between two independent methods of calculating CDR in our mesocosm systems, with a systematic offset (**Figure 4a**). The conventional approach used, measuring cation reaction products in exchange/solute pools, yielded mean CDR estimates of 0.80 ± 0.21 tCO₂eq ha⁻¹ (NPK-fertilized) and 0.43 ± 0.19 tCO₂eq ha⁻¹ (manure-fertilized) across all mesocosms. The TiCAT approach introduced here, measuring cation loss from the solid phase, gave mean CDR estimates of 1.34 ± 0.53 tCO₂eq ha⁻¹ (NPK-fertilized) and 0.78 ± 0.47 tCO₂eq ha⁻¹ (manure-fertilized). Mean CDR estimates from these methods were within standard error for both NPK- and manure-fertilized basalt-amended mesocosms. Additionally, some offset between

TiCAT and dissolved-pools estimates are not unexpected given the challenges of obtaining representative samples from the dissolved pools.

Mean initial CDR values across all basalt-amended mesocosms were 1.06 ± 0.50 tCO₂eq ha⁻¹ (TiCAT), and 0.61 ± 0.20 tCO₂eq ha⁻¹ (dissolved pools) (**Figure 4b**). This is broadly consistent with estimated CDR values calculated for similar ERW studies (see 25). Analysis of total inorganic carbon (TIC) and ammonium acetate leaching strongly suggest that carbonate formation and exchangeable cations in basalt feedstock should have a negligible impact on the overall cation budget of the mesocosm systems (*Supplementary Information*). Our results thus demonstrate that the solid-phase approach underlying TiCAT produces estimates for initial CDR within error of those calculated by analyzing the dissolved, plant and soil exchangeable pools that constitute the ultimate reaction products in our mesocosm experiments, suggesting that it can yield an accurate and robust estimate of initial CDR in enhanced weathering systems.

The TiCAT method overcomes significant issues with prior methods of estimating ERW, particularly those that rely on accurately measuring the amount and transport of weathering reaction products over time after feedstock application. Methods that rely on tracking the dissolved phase are extremely time- and labor-intensive, introducing potential barriers to scale. For example, a thorough study of a field-scale ERW trial monitoring aqueous reaction products, such as that conducted by ref. 54, involves many months of labor- and time-intensive sampling not only of soils, plants, and possibly porewaters from the agricultural plots onto which ERW feedstock is applied, but also a wider detailed monitoring of the drainage regime and watershed around such a site. Even using this style of sampling protocol, the necessary granularity of measurements would likely miss short-term fluctuations such as wash-out after rain events, which in many river systems account for an important component of the overall solute discharge (e.g., 97). Such measurements can also be complicated by varying timeframes over which cations are bound to exchangeable sorption sites within a soil (see 46, 47).

Our approach also overcomes possibly the largest uncertainty in scaling ERW within agricultural settings — estimating the initial extent of feedstock dissolution (see e.g., 33; 55). There is currently significant uncertainty on how surface areas will evolve through time within a given field setting (i.e., individual farm), and the extent to which secondary mineral formation on the surface of feedstock has the potential to alter mineral dissolution rates (e.g., 98-106). In addition, mineral dissolution kinetics are in some cases poorly constrained (e.g., 102, 107, 108). Taken together, these considerations make it challenging to accurately forecast feedstock dissolution across a range of deployment regimes with existing reaction-transport codes alone (33, 55, 98-108).

A significant additional advantage to this MRV approach is that it can directly integrate into existing agronomic practices. Gridded, pooled samples (109, 110) from the uppermost portion of the soil are already regularly taken for nutrient and soil pH analysis. Importantly, this means that there is already extensive personnel and infrastructure in place that can be leveraged to scale empirical validation of carbon capture through ERW at minimal cost, in marked contrast to empirical verification of soil organic carbon concentrations (SOC), which requires modified sampling protocols for accurate empirical results. Existing frameworks for carbon storage in agricultural settings are mostly focused on SOC (e.g., the US Department of Agriculture's COMET-Farm calculator, see <http://www.comet-farm.com>), which does not allow for landowners

and land users to include alkalinity generation through practices such as ERW into an estimate of carbon storage. Should ERW be deployed at scale, MRV tools such as TiCAT could be incorporated into these frameworks, which ideally allowing for synergistic use of ERW and soil organic carbon maintenance to achieve maximum carbon storage depending on local conditions.

It is important to emphasize that the value for CDR calculated based on the time-integrated amount of feedstock dissolution and cation loss should be regarded as an initial CDR value. There is potential for some amount of “leakage” of initially captured carbon downstream of a given field deployment, as alkalinity and dissolved organic carbon migrate from the soil through the transport continuum to the oceans (e.g., 20, 57). In addition, a large fraction of the dissolved cation load in any soil will be hosted, albeit transiently, in soil exchange sites (e.g., 111-113; see also 51). This cation storage at exchange sites is temporary, and upon their release dissolved cations will drive CDR through charge balance in the carbonic acid system (see 46, 47). However, there is a time-varying “lag” between feedstock dissolution and CO₂ capture that needs to be considered for accurate CDR quantification. A robust MRV approach with TiCAT at its core will also require modeling the transport of weathering products through the soil (14, 19, 43) and river-ocean system (20) to determine potential leakage through re-release of CO₂ back to the atmosphere.

Effective implementation of the TiCAT approach relies on stringent constraints on analytical error, which may be challenging via standard practice with most commercially available ICP-MS measurements (see 91, 92). Nonetheless, here, we have demonstrated that it is possible using isotope dilution on a standard quadrupole ICP-MS instrument to minimize analytical error to ~1%, making even <10% basalt dissolution analytically resolvable for total feedstock application rates of 50 t ha⁻¹. However, replication of this analytical precision in commercial laboratories will require adjustment to workflows and standard operating procedures. It is also likely that the aggregate impact on unit cost (dollar cost per ton of CO₂ captured) of TiCAT as an MRV procedure will broadly follow a “learning curve” trajectory (e.g., 114).

5 Conclusion

We have demonstrated with mesocosm experiments that a soil-based mass balance approach to track ERW with a basalt feedstock — TiCAT — yields CDR estimates that are within error of those calculated by monitoring the gain of weathering products across mesocosm cation pools. Using an isotope dilution method, we can reduce analytical error sufficiently that a dissolution signal is resolvable in the solid soil phase at reasonable feedstock application rates. In mesocosm experiments, all reaction products can be tracked and measured with a high degree of certainty. Applying the methods used in this study to field-scale trials is a necessary next step in verifying the capacity of TiCAT to be used for MRV in ERW in the field, and the approach described here will ultimately need to be augmented by the development of cradle-to-grave MRV approaches that can provide error-bounded estimates of final CDR. Nevertheless, our results suggest that the TiCAT method has the potential to be a cost-effective and accurate centerpiece of a robust MRV toolkit for deploying ERW at scale.

Figures

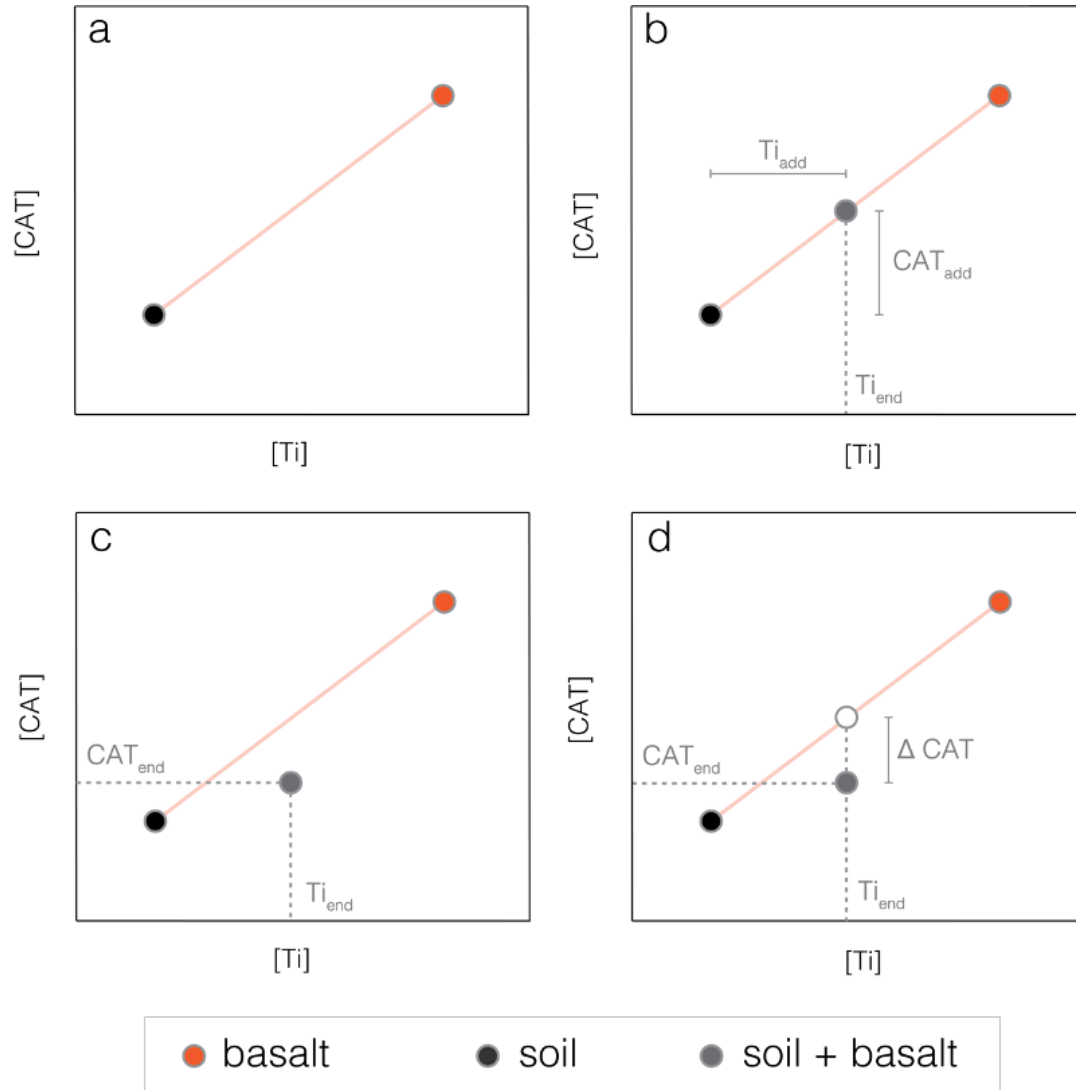


Figure 1. The TiCAT conceptual framework as a simple two-component mixing model. An idealized soil and basalt endmember are plotted in Ti v CAT space (a). A mixture of soil+basalt initially plots on the idealized mixing line between both endmembers (b). Dissolution results in loss of CAT from the solid phase, while Ti is conserved as it is immobile (c). The original composition of the soil+basalt mixture (indicated by the white circle) is the intersection of Ti_{end} with the mixing line; ΔCAT is the amount of CAT lost by dissolution (d).

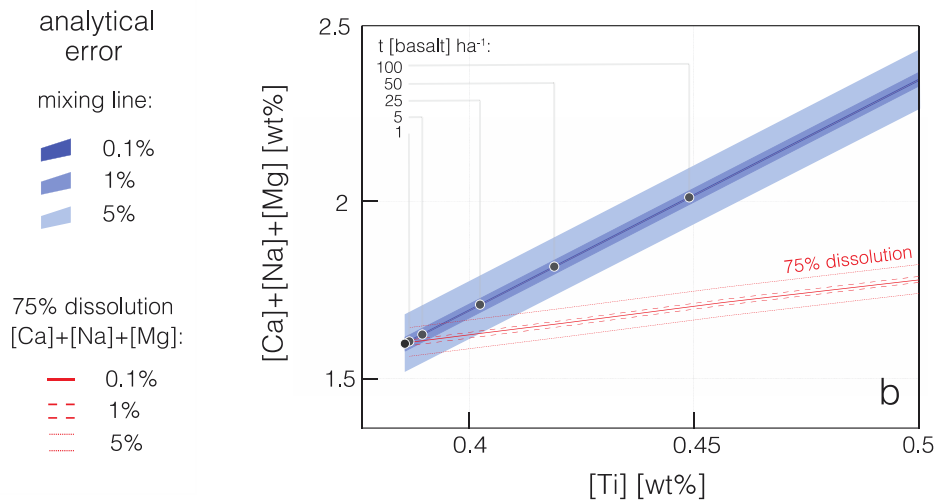
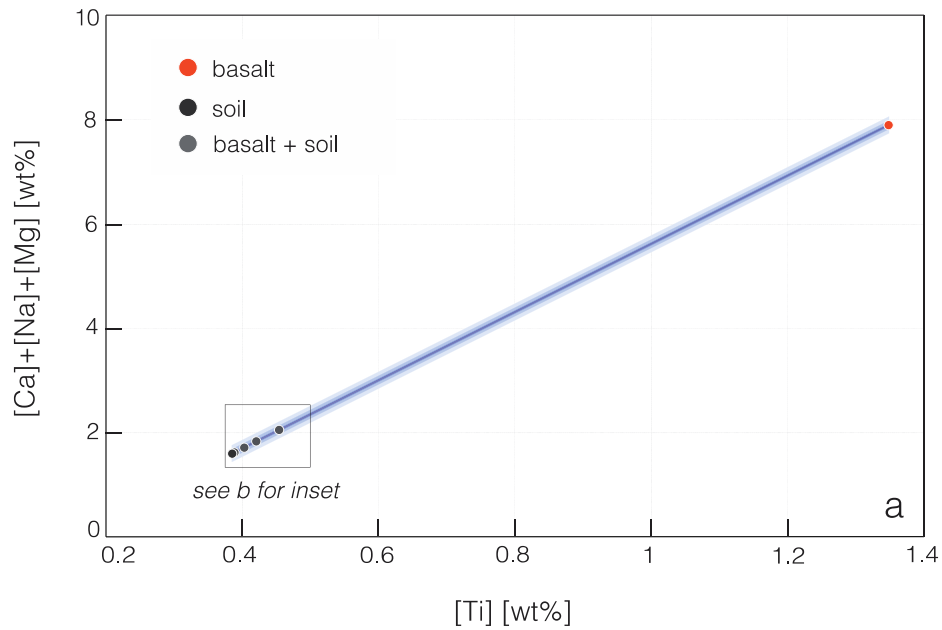


Figure 2. A mixing model with representative data for soil and basalt endmembers. Assumed homogeneous mixtures of basalt+soil are shown, for a range of basalt application scenarios (see inset, b). Error envelopes are shown for mixing line and a line indicating theoretical 75% dissolution, based on potential size of analytical error on basalt+soil samples. Resolvability of a dissolution signal is dependent on dissolution rate, basalt application rate, and analytical error.

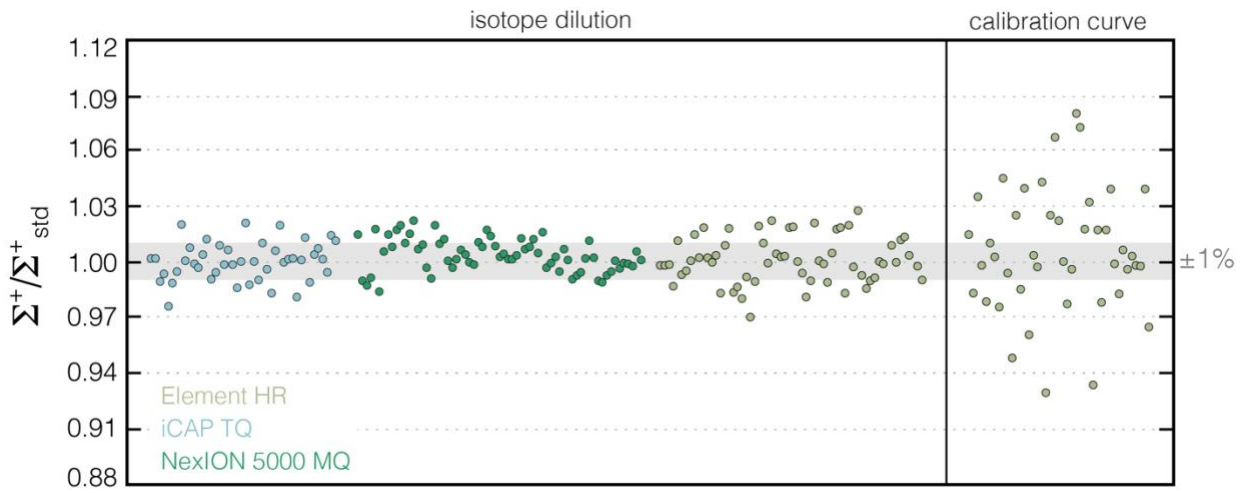


Figure 3. Representative analytical error on standards run on three models of ICP-MS, using calibration curve method and isotope dilution method. The grey shaded region represents an analytical error range of $\pm 1\%$.

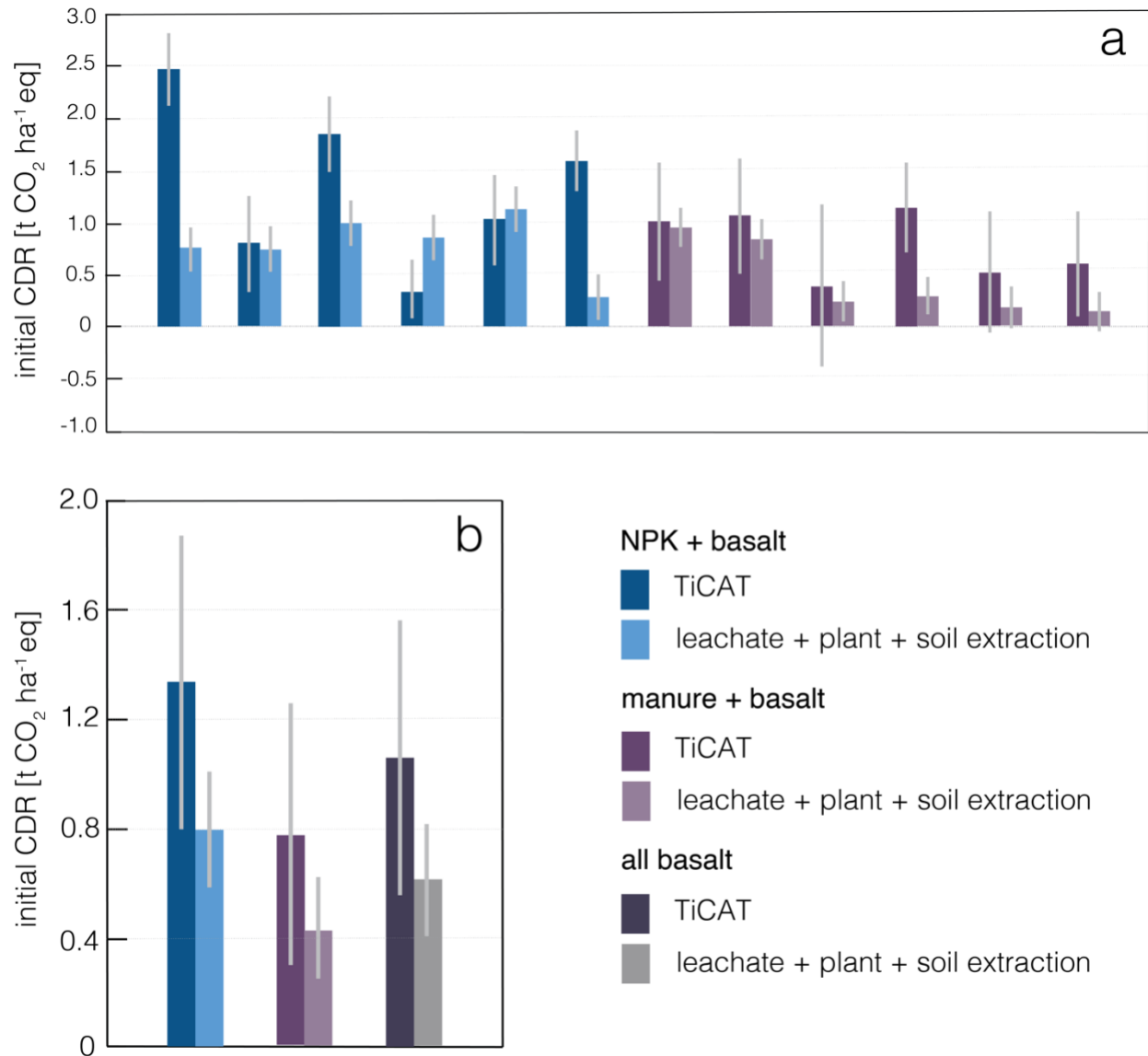


Figure 4. Initial CDR estimates for in this study, calculated using cation data from TiCAT and non-mineral-bound pools. Results are shown for individual mesocosms (a), and as mean values for all mesocosms pooled by treatment type, where grey bars show all basalt-treated columns as a single pooled data set (b). Error bars for TiCAT are propagated analytical error and standard error where baseline soil and basalt samples have been pooled; error bars for leachate + plant + soil extraction are standard error from control columns used as baseline.

Acknowledgments

NJP acknowledges support from the Yale Center for Natural Carbon Capture. DJB acknowledges funding from the Leverhulme Centre for Climate Change Mitigation.

References

1. Ou, Y., Iyer, G., Clarke, L., Edmonds, J., Fawcett, A.A., Hultman, N., McFarland, J.R., Binsted, M., Cui, R., Fyson, C., Geiges, A., Gonzales-Zuñiga, S., Gidden, M.J., Höhne, N., Jeffery, L., Kuramochi, T., Lewis, J., Meinshausen, M., Nicholls, Z., Patel, P., Ragnauth, S., Rogelj, J., Waldhoff, S., Yu, S., McJeon, H., 2021. Can updated climate pledges limit warming well below 2°C? *Science* 374, 693–695. <https://doi.org/10.1126/science.abl8976>
2. Meinshausen, M., Lewis, J., McGlade, C., Gütschow, J., Nicholls, Z., Burdon, R., Cozzi, L., Hackmann, B., 2022. Realization of Paris Agreement pledges may limit warming just below 2 °C. *Nature* 604, 304–309. <https://doi.org/10.1038/s41586-022-04553-z>
3. United Nations Environment Programme, 2022. Emissions Gap Report 2022: The Closing Window — Climate crisis calls for rapid transformation of societies. Nairobi. <https://www.unep.org/emissions-gap-report-2022>
4. Lawrence, M.G., Schäfer, S., Muri, H., Scott, V., Oschlies, A., Vaughan, N.E., Boucher, O., Schmidt, H., Haywood, J., Scheffran, J., 2018. Evaluating climate geoengineering proposals in the context of the Paris Agreement temperature goals. *Nat Commun* 9, 3734. <https://doi.org/10.1038/s41467-018-05938-3>
5. IPCC, 2022. *Climate Change 2022: Mitigation of Climate Change. Contribution of Working Group III to the Sixth Assessment Report of the Intergovernmental Panel on Climate Change* [P.R. Shukla, J. Skea, R. Slade, A. Al Khourdajie, R. van Diemen, D. McCollum, M. Pathak, S. Some, P. Vyas, R. Fradera, M. Belkacemi, A. Hasija, G. Lisboa, S. Luz, J. Malley, (eds.)]. Cambridge University Press, Cambridge, UK and New York, NY, USA. doi: 10.1017/9781009157926
6. Schuiling, R.D., Krijgsman, P., 2006. Enhanced Weathering: An Effective and Cheap Tool to Sequester Co₂. *Climatic Change* 74, 349–354. <https://doi.org/10.1007/s10584-005-3485-y>
7. Köhler, P., Hartmann, J., Wolf-Gladrow, D.A., 2010. Geoengineering potential of artificially enhanced silicate weathering of olivine. *Proc National Acad Sci* 107, 20228–20233. <https://doi.org/10.1073/pnas.1000545107>
8. Renforth, P., 2012. The potential of enhanced weathering in the UK. *Int J Greenh Gas Con* 10, 229–243. <https://doi.org/10.1016/j.ijggc.2012.06.011>
9. [Hartmann, J., West, A.J., Renforth, P., Köhler, P., Rocha, C.L.D.L., Wolf-Gladrow, D.A., Dürr, H.H., Scheffran, J., 2013. Enhanced chemical weathering as a geoengineering strategy to reduce atmospheric carbon dioxide, supply nutrients, and mitigate ocean acidification. *Rev Geophys* 51, 113–149. <https://doi.org/10.1002/rog.20004>](https://doi.org/10.1016/j.ijggc.2012.06.011)

10. Kantola, I.B., Masters, M.D., Beerling, D.J., Long, S.P., DeLucia, E.H., 2017. Potential of global croplands and bioenergy crops for climate change mitigation through deployment for enhanced weathering. *Biol Letters* 13, 20160714. <https://doi.org/10.1098/rsbl.2016.0714>
11. Taylor, L.L., Beerling, D.J., Quegan, S., Banwart, S.A., 2017. Simulating carbon capture by enhanced weathering with croplands: an overview of key processes highlighting areas of future model development. *Biol Letters* 13, 20160868. <https://doi.org/10.1098/rsbl.2016.0868>
12. Strefler, J., Amann, T., Bauer, N., Kriegler, E., Hartmann, J., 2018. Potential and costs of carbon dioxide removal by enhanced weathering of rocks. *Environ Res Lett* 13, 034010. <https://doi.org/10.1088/1748-9326/aaa9c4>
13. Beerling, D.J., Leake, J.R., Long, S.P., Scholes, J.D., Ton, J., Nelson, P.N., Bird, M., Kantzas, E., Taylor, L.L., Sarkar, B., Kelland, M., DeLucia, E., Kantola, I., Müller, C., Rau, G., Hansen, J., 2018. Farming with crops and rocks to address global climate, food and soil security. *Nat Plants* 4, 138–147. <https://doi.org/10.1038/s41477-018-0108-y>
14. Beerling, D.J., Kantzas, E.P., Lomas, M.R., Wade, P., Eufrazio, R.M., Renforth, P., Sarkar, B., Andrews, M.G., James, R.H., Pearce, C.R., Mercure, J.-F., Pollitt, H., Holden, P.B., Edwards, N.R., Khanna, M., Koh, L., Quegan, S., Pidgeon, N.F., Janssens, I.A., Hansen, J., Banwart, S.A., 2020. Potential for large-scale CO₂ removal via enhanced rock weathering with croplands. *Nature* 583, 242–248. <https://doi.org/10.1038/s41586-020-2448-9>
15. Taylor, L.L., Quirk, J., Thorley, R.M.S., Kharecha, P.A., Hansen, J., Ridgwell, A., Lomas, M.R., Banwart, S.A., Beerling, D.J., 2016. Enhanced weathering strategies for stabilizing climate and averting ocean acidification. *Nat Clim Change* 6, 402–406. <https://doi.org/10.1038/nclimate2882>
16. Edwards, D.P., Lim, F., James, R.H., Pearce, C.R., Scholes, J., Freckleton, R.P., Beerling, D.J., 2017. Climate change mitigation: potential benefits and pitfalls of enhanced rock weathering in tropical agriculture. *Biol Letters* 13, 20160715. <https://doi.org/10.1098/rsbl.2016.0715>
17. Goll, D.S., Ciais, P., Amann, T., Buermann, W., Chang, J., Eker, S., Hartmann, J., Janssens, I., Li, W., Obersteiner, M., Penuelas, J., Tanaka, K., Vicca, S., 2021. Potential CO₂ removal from enhanced weathering by ecosystem responses to powdered rock. *Nat Geosci* 14, 545–549. <https://doi.org/10.1038/s41561-021-00798-x>
18. Rinder, T., von Hagke, C., 2021. [The influence of particle size on the potential of enhanced basalt weathering for carbon dioxide removal - Insights from a regional assessment](https://doi.org/10.1016/j.jclepro.2021.128178). *J Clean Prod* 315, 128178. <https://doi.org/10.1016/j.jclepro.2021.128178>

19. Kantzas, E.P., Martin, M.V., Lomas, M.R., Eufrazio, R.M., Renforth, P., Lewis, A.L., Taylor, L.L., Mecure, J.-F., Pollitt, H., Vercoulen, P.V., Vakilifard, N., Holden, P.B., Edwards, N.R., Koh, L., Pidgeon, N.F., Banwart, S.A., Beerling, D.J., 2022. Substantial carbon drawdown potential from enhanced rock weathering in the United Kingdom. *Nat Geosci* 15, 382–389. <https://doi.org/10.1038/s41561-022-00925-2>
20. Zhang, S., Planavsky, N.J., Katchinoff, J., Raymond, P.A., Kanzaki, Y., Reershemius, T., Reinhard, C.T., 2022. River chemistry constraints on the carbon capture potential of surficial enhanced rock weathering. *Limnol Oceanogr.* <https://doi.org/10.1002/lno.12244>
21. Middelburg, J. J., Soetaert, K., Hagens, M., 2020. Ocean Alkalinity, Buffering and Biogeochemical Processes. *Reviews of Geophysics*, 58(3), e2019RG000681. <https://doi.org/10.1029/2019rg000681>
22. Urey, H. C., 1952. On the Early Chemical History of the Earth and the Origin of Life. *Proceedings of the National Academy of Sciences*, 38(4), 351–363. <https://doi.org/10.1073/pnas.38.4.351>
23. Berner, R. A., Lasaga, A. C., Garrels, R. M., 1983. The carbonate-silicate geochemical cycle and its effect on atmospheric carbon dioxide over the past 100 million years. *American Journal of Science*, 283(7), 641–683. <https://doi.org/10.2475/ajs.283.7.641>
24. Isson, T. T., Planavsky, N. J., Coogan, L. A., Stewart, E. M., Ague, J. J., Bolton, E. W., Zhang, S., McKenzie, N. R., Kump, L. R., 2020. Evolution of the Global Carbon Cycle and Climate Regulation on Earth. *Global Biogeochemical Cycles*, 34(2). <https://doi.org/10.1029/2018gb006061>
25. Smith, P., 2016. Soil carbon sequestration and biochar as negative emission technologies. *Global Change Biol* 22, 1315–1324. <https://doi.org/10.1111/gcb.13178>
26. Schlesinger, W.H., Amundson, R., 2019. Managing for soil carbon sequestration: Let's get realistic. *Global Change Biol* 25, 386–389. <https://doi.org/10.1111/gcb.14478>
27. Bossio, D.A., Cook-Patton, S.C., Ellis, P.W., Fargione, J., Sanderman, J., Smith, P., Wood, S., Zomer, R.J., Unger, M. von, Emmer, I.M., Griscom, B.W., 2020. The role of soil carbon in natural climate solutions. *Nat Sustain* 3, 391–398. <https://doi.org/10.1038/s41893-020-0491-z>
28. ten Berge, H.F.M., Meer, H.G. van der, Steenhuizen, J.W., Goedhart, P.W., Knops, P., Verhagen, J., 2012. Olivine Weathering in Soil, and Its Effects on Growth and Nutrient Uptake in Ryegrass (*Lolium perenne* L.): A Pot Experiment. *Plos One* 7, e42098. <https://doi.org/10.1371/journal.pone.0042098>
29. Song, Z., Liu, C., Müller, K., Yang, X., Wu, Y., Wang, H., 2018. Silicon regulation of soil organic carbon stabilization and its potential to mitigate climate change. *Earth-sci Rev* 185, 463–475. <https://doi.org/10.1016/j.earscirev.2018.06.020>

30. Amann, T., Hartmann, J., Struyf, E., Garcia, W. de O., Fischer, E.K., Janssens, I., Meire, P., Schoelynck, J., 2020. Enhanced Weathering and related element fluxes – a cropland mesocosm approach. *Biogeosciences* 17, 103–119. <https://doi.org/10.5194/bg-17-103-2020>
31. Garcia, W. de O., Amann, T., Hartmann, J., Karstens, K., Popp, A., Boysen, L.R., Smith, P., Goll, D., 2020. Impacts of enhanced weathering on biomass production for negative emission technologies and soil hydrology. *Biogeosciences* 17, 2107–2133. <https://doi.org/10.5194/bg-17-2107-2020>
32. Kelland, M.E., Wade, P.W., Lewis, A.L., Taylor, L.L., Sarkar, B., Andrews, M.G., Lomas, M.R., Cotton, T.E.A., Kemp, S.J., James, R.H., Pearce, C.R., Hartley, S.E., Hodson, M.E., Leake, J.R., Banwart, S.A., Beerling, D.J., 2020. Increased yield and CO₂ sequestration potential with the C₄ cereal *Sorghum bicolor* cultivated in basaltic rock dust-amended agricultural soil. *Global Change Biol* 26, 3658–3676. <https://doi.org/10.1111/gcb.15089>
33. Swoboda, P., Döring, T.F., Hamer, M., 2021. Remineralizing soils? The agricultural usage of silicate rock powders: A review. *Sci Total Environ* 807, 150976. <https://doi.org/10.1016/j.scitotenv.2021.150976>
34. Davies, B., Finney, B., Eagle, D., 2001. Resource Management: Soil. Farming Press, ISBN 0 85236 559 4.
35. Kamprath, E.J., Smyth, T.J., 2005. Liming. In: Hillel, D. (ed.). Encyclopedia of Soils in the Environment. Elsevier, ISBN 9780123485304, 350-358. <https://doi.org/10.1016/B0-12-348530-4/00225-3>
36. Goulding, K.W.T., 2016. Soil acidification and the importance of liming agricultural soils with particular reference to the United Kingdom. *Soil Use Manage*, 32: 390-399. <https://doi.org/10.1111/sum.12270>
37. Semhi, K., Suchet, P.A., Clauer, N., Probst, J.-L., 2000. Impact of nitrogen fertilizers on the natural weathering-erosion processes and fluvial transport in the Garonne basin. *Appl Geochem* 15, 865–878. [https://doi.org/10.1016/s0883-2927\(99\)00076-1](https://doi.org/10.1016/s0883-2927(99)00076-1)
38. West, T.O., McBride, A.C., 2005. The contribution of agricultural lime to carbon dioxide emissions in the United States: dissolution, transport, and net emissions. *Agric Ecosyst Environ* 108, 145–154. <https://doi.org/10.1016/j.agee.2005.01.002>
39. Oh, N., Raymond, P.A., 2006. Contribution of agricultural liming to riverine bicarbonate export and CO₂ sequestration in the Ohio River basin. *Global Biogeochem Cy* 20, n/a-n/a. <https://doi.org/10.1029/2005gb002565>

40. Hamilton, S.K., Kurzman, A.L., Arango, C., Jin, L., Robertson, G.P., 2007. Evidence for carbon sequestration by agricultural liming. *Global Biogeochem Cy* 21, n/a-n/a. <https://doi.org/10.1029/2006gb002738>
41. Perrin, A.-S., Probst, A., Probst, J.-L., 2008. Impact of nitrogenous fertilizers on carbonate dissolution in small agricultural catchments: Implications for weathering CO₂ uptake at regional and global scales. *Geochim Cosmochim Ac* 72, 3105–3123. <https://doi.org/10.1016/j.gca.2008.04.011>
42. Dietzen, C., Harrison, R., Michelsen-Correa, S., 2018. Effectiveness of enhanced mineral weathering as a carbon sequestration tool and alternative to agricultural lime: An incubation experiment. *Int J Greenh Gas Con* 74, 251–258. <https://doi.org/10.1016/j.ijggc.2018.05.007>
43. Kanzaki, Y., Zhang, S., Planavsky, N.J., Reinhard, C.T., 2022. Soil Cycles of Elements simulator for Predicting TERrestrial regulation of greenhouse gases: SCEPTER v0.9. *Geoscientific Model Dev Discuss* 2022, 1–58. <https://doi.org/10.5194/gmd-2022-8>
44. Cipolla, G., Calabrese, S., Noto, L.V., Porporato, A., 2021. The role of hydrology on enhanced weathering for carbon sequestration I. Modeling rock-dissolution reactions coupled to plant, soil moisture, and carbon dynamics. *Adv Water Resour* 154, 103934. <https://doi.org/10.1016/j.advwatres.2021.103934>
45. Renforth, P., Pogge von Strandmann, P.A.E., Henderson, G.M., 2015. The dissolution of olivine added to soil: Implications for enhanced weathering. *Appl Geochem* 61, 109–118. <https://doi.org/10.1016/j.apgeochem.2015.05.016>
46. Pogge von Strandmann, P.A.E, Fraser, W.T., Hammond, S.J., Tarbuck, G., Wood, I.G., Oelkers, E.H., Murphy, M.J., 2019. Experimental determination of Li isotope behaviour during basalt weathering. *Chem Geol* 517, 34–43. <https://doi.org/10.1016/j.chemgeo.2019.04.020>
47. Pogge von Strandmann, P.A.E., Renforth, P., West, A.J., Murphy, M.J., Luu, T.-H., Henderson, G.M., 2021. The lithium and magnesium isotope signature of olivine dissolution in soil experiments. *Chem Geol* 560, 120008. <https://doi.org/10.1016/j.chemgeo.2020.120008>
48. Pogge von Strandmann, P.A.E, Tooley, C., Mulders, J.J.P.A., Renforth, P., 2022. The Dissolution of Olivine Added to Soil at 4°C: Implications for Enhanced Weathering in Cold Regions. *Frontiers Clim* 4. <https://doi.org/10.3389/fclim.2022.827698>
49. Amann, T., Hartmann, J., Hellmann, R., Pedrosa, E.T., Malik, A., 2022. Enhanced weathering potentials—the role of in situ CO₂ and grain size distribution. *Frontiers Clim* 4, 929268. <https://doi.org/10.3389/fclim.2022.929268>

50. Jariwala, H., Haque, F., Vanderburgt, S., Santos, R.M., Chiang, Y.W., 2022. Mineral–Soil–Plant–Nutrient Synergisms of Enhanced Weathering for Agriculture: Short-Term Investigations Using Fast-Weathering Wollastonite Skarn. *Front Plant Sci* 13, 929457. <https://doi.org/10.3389/fpls.2022.929457>
51. Vienne, A., Poblador, S., Portillo-Estrada, M., Hartmann, J., Ijehon, S., Wade, P., Vicca, S., 2022. Enhanced Weathering Using Basalt Rock Powder: Carbon Sequestration, Co-benefits and Risks in a Mesocosm Study With *Solanum tuberosum*. *Frontiers Clim* 4, 869456. <https://doi.org/10.3389/fclim.2022.869456>
52. Haque, F., Santos, R.M., Chiang, Y.W., 2020. CO₂ sequestration by wollastonite-amended agricultural soils – An Ontario field study. *Int J Greenh Gas Con* 97, 103017. <https://doi.org/10.1016/j.ijggc.2020.103017>
53. Taylor, L.L., Driscoll, C.T., Groffman, P.M., Rau, G.H., Blum, J.D., Beerling, D.J., 2021. Increased carbon capture by a silicate-treated forested watershed affected by acid deposition. *Biogeosciences* 18, 169–188. <https://doi.org/10.5194/bg-18-169-2021>
54. Larkin, C.S., Andrews, M.G., Pearce, C.R., Yeong, K.L., Beerling, D.J., Bellamy, J., Benedick, S., Freckleton, R.P., Goring-Harford, H., Sadekar, S., James, R.H., 2022. Quantification of CO₂ removal in a large-scale enhanced weathering field trial on an oil palm plantation in Sabah, Malaysia. *Frontiers Clim* 4, 959229. <https://doi.org/10.3389/fclim.2022.959229>
55. Calabrese, S., Wild, B., Bertagni, M.B., Bourg, I.C., White, C., Aburto, F., Cipolla, G., Noto, L.V., Porporato, A., 2022. Nano- to Global-Scale Uncertainties in Terrestrial Enhanced Weathering. *Environ Sci Technol*. <https://doi.org/10.1021/acs.est.2c03163>
56. Almaraz, M., Bingham, N.L., Holzer, I.O., Geoghegan, E.K., Goertzen, H., Sohng, J., Houlton, B.Z., 2022. Methods for determining the CO₂ removal capacity of enhanced weathering in agronomic settings. *Frontiers Clim* 4, 970429. <https://doi.org/10.3389/fclim.2022.970429>
57. Chay, F., Klitzke, J., Hausfather, Z., Martin, K., Freeman, J., Cullenward, D., 2022. Verification Confidence Levels for carbon dioxide removal. *CarbonPlan* <https://carbonplan.org/research/cdr-verification-explainer>
58. Brimhall, G.H., Dietrich, W.E., 1987. Constitutive mass balance relations between chemical composition, volume, density, porosity, and strain in metasomatic hydrochemical systems: Results on weathering and pedogenesis. *Geochim Cosmochim Ac* 51, 567–587. [https://doi.org/10.1016/0016-7037\(87\)90070-6](https://doi.org/10.1016/0016-7037(87)90070-6)
59. Chadwick, O.A., Brimhall, G.H., Hendricks, D.M., 1990. From a black to a gray box — a mass balance interpretation of pedogenesis. *Geomorphology* 3, 369–390. [https://doi.org/10.1016/0169-555x\(90\)90012-f](https://doi.org/10.1016/0169-555x(90)90012-f)

60. Chadwick, O.A., Derry, L.A., Vitousek, P.M., Huebert, B.J., Hedin, L.O., 1999. Changing sources of nutrients during four million years of ecosystem development. *Nature* 397, 491–497. <https://doi.org/10.1038/17276>
61. Brimhall, G.H., J., L.C., Ford, C., Bratt, J., Taylor, G., Warin, O., 1991. Quantitative geochemical approach to pedogenesis: importance of parent material reduction, volumetric expansion, and eolian influx in lateritization. *Geoderma* 51, 51–91. [https://doi.org/10.1016/0016-7061\(91\)90066-3](https://doi.org/10.1016/0016-7061(91)90066-3)
62. Kurtz, A.C., Derry, L.A., Chadwick, O.A., Alfano, M.J., 2000. Refractory element mobility in volcanic soils. *Geology* 28, 683–686. [https://doi.org/10.1130/0091-7613\(2000\)28<683:remivs>2.0.co;2](https://doi.org/10.1130/0091-7613(2000)28<683:remivs>2.0.co;2)
63. White, A.F., Bullen, T.D., Schulz, M.S., Blum, A.E., Huntington, T.G., Peters, N.E., 2001. Differential rates of feldspar weathering in granitic regoliths. *Geochim Cosmochim Acta* 65, 847–869. [https://doi.org/10.1016/s0016-7037\(00\)00577-9](https://doi.org/10.1016/s0016-7037(00)00577-9)
64. Anderson, S.P., Dietrich, W.E., Brimhall, G.H., 2002. Weathering profiles, mass-balance analysis, and rates of solute loss: Linkages between weathering and erosion in a small, steep catchment. *Gsa Bulletin* 114, 1143–1158. [https://doi.org/10.1130/0016-7606\(2002\)114<1143:wpmbaa>2.0.co;2](https://doi.org/10.1130/0016-7606(2002)114<1143:wpmbaa>2.0.co;2)
65. Riebe, C.S., Kirchner, J.W., Finkel, R.C., 2003. Long-term rates of chemical weathering and physical erosion from cosmogenic nuclides and geochemical mass balance. *Geochim Cosmochim Acta* 67, 4411–4427. [https://doi.org/10.1016/s0016-7037\(03\)00382-x](https://doi.org/10.1016/s0016-7037(03)00382-x)
66. Tabor, N.J., Montañez, I.P., Zierenberg, R., Currie, B.S., 2004. Mineralogical and geochemical evolution of a basalt-hosted fossil soil (Late Triassic, Ischigualasto Formation, northwest Argentina): Potential for paleoenvironmental reconstruction. *Gsa Bulletin* 116, 1280–1293. <https://doi.org/10.1130/b25222.1>
67. Sheldon, N.D., Tabor, N.J., 2009. Quantitative paleoenvironmental and paleoclimatic reconstruction using paleosols. *Earth-sci Rev* 95, 1–52. <https://doi.org/10.1016/j.earscirev.2009.03.004>
68. Brantley, S.L., Lebedeva, M., 2011. Learning to Read the Chemistry of Regolith to Understand the Critical Zone. *Annu Rev Earth Pl Sc* 39, 387–416. <https://doi.org/10.1146/annurev-earth-040809-152321>
69. Fisher, B.A., Rendahl, A.K., Aufdenkampe, A.K., Yoo, K., 2017. Quantifying weathering on variable rocks, an extension of geochemical mass balance: Critical zone and landscape evolution. *Earth Surf. Process. Landforms* 42, 2457–2468. <https://doi.org/10.1002/esp.4212>
70. Lipp, A.G., Shorttle, O., Sperling, E.A., Brocks, J.J., Cole, D.B., Crockford, P.W., Mouro, L.D., Dewing, K., Dornbos, S.Q., Emmings, J.F., Farrell, U.C., Jarrett, A.,

Johnson, B.W., Kabanov, P., Keller, C.B., Kunzmann, M., Miller, A.J., Mills, N.T., O'Connell, B., Peters, S.E., Planavsky, N.J., Ritzer, S.R., Schoepfer, S.D., Wilby, P.R., Yang, J., 2021. The composition and weathering of the continents over geologic time. *Geochem Perspectives Lett* 21–26. <https://doi.org/10.7185/geochemlet.2109>

71. Monro, S.K., Loughnan, F.C., and Walker, M.C., 1983, The Ayrshire bauxitic clay: An allochthonous deposit?, in Wilson, R.C.L., ed., Residual deposits: Geological Society (London) Special Publication 11, p. 47–58
72. Middelburg, J.J., Weijden, C.H. van der, Woittiez, J.R.W., 1988. Chemical processes affecting the mobility of major, minor and trace elements during weathering of granitic rocks. *Chem Geol* 68, 253–273. [https://doi.org/10.1016/0009-2541\(88\)90025-3](https://doi.org/10.1016/0009-2541(88)90025-3)
73. Tilley, D.B., Eggleton, R.A., 2005. Titanite Low-Temperature Alteration and Ti Mobility. *Clay Clay Miner* 53, 100–107. <https://doi.org/10.1346/ccmn.2005.0530110>
74. Taboada, T., Cortizas, A.M., García, C., García-Rodeja, E., 2006. Particle-size fractionation of titanium and zirconium during weathering and pedogenesis of granitic rocks in NW Spain. *Geoderma* 131, 218–236. <https://doi.org/10.1016/j.geoderma.2005.03.025>
75. Du, X., Rate, A.W., Gee, M.A.M., 2012. Redistribution and mobilization of titanium, zirconium and thorium in an intensely weathered lateritic profile in Western Australia. *Chem Geol* 330, 101–115. <https://doi.org/10.1016/j.chemgeo.2012.08.030>
76. Langmuir, D., Herman, J.S., 1980. The mobility of thorium in natural waters at low temperatures. *Geochim Cosmochim Acta* 44, 1753–1766. [https://doi.org/10.1016/0016-7037\(80\)90226-4](https://doi.org/10.1016/0016-7037(80)90226-4)
77. Braun, J.-J., Pagel, M., Herbilln, A., Rosin, C., 1993. Mobilization and redistribution of REEs and thorium in a syenitic lateritic profile: A mass balance study. *Geochim Cosmochim Acta* 57, 4419–4434. [https://doi.org/10.1016/0016-7037\(93\)90492-f](https://doi.org/10.1016/0016-7037(93)90492-f)
78. Little, M.G., Lee, C.-T.A., 2010. Sequential extraction of labile elements and chemical characterization of a basaltic soil from Mt. Meru, Tanzania. *J Afr Earth Sci* 57, 444–454. <https://doi.org/10.1016/j.jafrearsci.2009.12.001>
79. Jiang, K., Qi, H.-W., Hu, R.-Z., 2018. Element mobilization and redistribution under extreme tropical weathering of basalts from the Hainan Island, South China. *J Asian Earth Sci* 158, 80–102. <https://doi.org/10.1016/j.jseaes.2018.02.008>
80. Nesbitt, H.W., 1979. Mobility and fractionation of rare earth elements during weathering of a granodiorite. *Nature* 279, 206–210. <https://doi.org/10.1038/279206a0>
81. Gouveia, M.A., Prudêncio, M.I., Figueiredo, M.O., Pereira, L.C.J., Waerenborgh, J.C., Morgado, I., Pena, T., Lopes, A., 1993. Behavior of REE and other trace and major

elements during weathering of granitic rocks, Évora, Portugal. *Chem Geol* 107, 293–296. [https://doi.org/10.1016/0009-2541\(93\)90194-n](https://doi.org/10.1016/0009-2541(93)90194-n)

82. Boulangé, B., Colin, F., 1994. Rare earth element mobility during conversion of nepheline syenite into lateritic bauxite at Passa Quatro, Minas Gerais, Brazil. *Appl Geochem* 9, 701–711. [https://doi.org/10.1016/0883-2927\(94\)90029-9](https://doi.org/10.1016/0883-2927(94)90029-9)
83. Öhlander, B., Land, M., Ingri, J., Widerlund, A., 1996. Mobility of rare earth elements during weathering of till in northern Sweden. *Appl Geochem* 11, 93–99. [https://doi.org/10.1016/0883-2927\(95\)00044-5](https://doi.org/10.1016/0883-2927(95)00044-5)
84. Tertre, E., Hofmann, A., Berger, G., 2008. Rare earth element sorption by basaltic rock: Experimental data and modeling results using the “Generalised Composite approach.” *Geochim Cosmochim Acta* 72, 1043–1056. <https://doi.org/10.1016/j.gca.2007.12.015>
85. Jain, J.C., Neal, C.R., Hanchar, J.M., 2001. Problems Associated with the Determination of Rare Earth Elements of a “Gem” Quality Zircon by Inductively Coupled Plasma-Mass Spectrometry. *Geostandard Newslett* 25, 229–237. <https://doi.org/10.1111/j.1751-908x.2001.tb00598.x>
86. Melfi, A.J., Subies, F., Nahon, D., Formoso, M.L.L., 1996. Zirconium mobility in bauxites of Southern Brazil. *J S Am Earth Sci* 9, 161–170. [https://doi.org/10.1016/0895-9811\(96\)00003-x](https://doi.org/10.1016/0895-9811(96)00003-x)
87. Cornu, S., Lucas, Y., Lebon, E., Ambrosi, J.P., Luizão, F., Rouiller, J., Bonnay, M., Neal, C., 1999. Evidence of titanium mobility in soil profiles, Manaus, central Amazonia. *Geoderma* 91, 281–295. [https://doi.org/10.1016/s0016-7061\(99\)00007-5](https://doi.org/10.1016/s0016-7061(99)00007-5)
88. Hill, I.G., Worden, R.H., Meighan, I.G., 2000. Yttrium: The immobility-mobility transition during basaltic weathering. *Geology* 28, 923–926. [https://doi.org/10.1130/0091-7613\(2000\)28<923:ytitdb>2.0.co;2](https://doi.org/10.1130/0091-7613(2000)28<923:ytitdb>2.0.co;2)
89. Hodson, M.E., 2002. Experimental evidence for mobility of Zr and other trace elements in soils. *Geochim Cosmochim Acta* 66, 819–828. [https://doi.org/10.1016/s0016-7037\(01\)00803-1](https://doi.org/10.1016/s0016-7037(01)00803-1)
90. Bednar, A.J., Gent, D.B., Gilmore, J.R., Sturgis, T.C., Larson, S.L., 2004. Mechanisms of Thorium Migration in a Semiarid Soil. *J Environ Qual* 33, 2070–2077. <https://doi.org/10.2134/jeq2004.2070>
91. Andersen, J.E.T., 2014. On the development of quality assurance. *Trac Trends Anal Chem* 60, 16–24. <https://doi.org/10.1016/j.trac.2014.04.016>
92. Eggen, O.A., Reimann, C., Flem, B., 2019. Reliability of geochemical analyses: Deja vu all over again. *Sci Total Environ* 670, 138–148. <https://doi.org/10.1016/j.scitotenv.2019.03.185>

93. Inghram, M.G., 1954. Stable isotope dilution as an analytical tool. *Ann Rev Nucl Sci* 4:1, 81-92. <https://doi.org/10.1146/annurev.ns.04.120154.000501>
94. Evans, E.H., Clough, R., 2005. Isotope dilution analysis. In: Worsfold, P., Townshend, A., Poole, C. (eds.). *Encyclopedia of Analytical Science* (2nd ed.). Elsevier, 545-553. <https://doi.org/10.1016/B0-12-369397-7/00301-0>
95. Stracke, A., Scherer, E.E., Reynolds, B.C., 2014. Application of isotope dilution in geochemistry. *Treatise on Geochemistry* (Second Edition) 71–86. <https://doi.org/10.1016/b978-0-08-095975-7.01404-2>
96. Willbold, M., Jochum, K.P., 2005. Multi-Element Isotope Dilution Sector Field ICP-MS: A Precise Technique for the Analysis of Geological Materials and its Application to Geological Reference Materials. *Geostand Geoanal Res* 29, 63–82. <https://doi.org/10.1111/j.1751-908x.2005.tb00656.x>
97. Raymond, P.A., Saiers, J.E., Sobczak, W.V., 2016. Hydrological and biogeochemical controls on watershed dissolved organic matter transport: pulse-shunt concept. *Ecology* 97, 5–16. <https://doi.org/10.1890/14-1684.1>
98. Siever, R., Woodford, N., 1979. Dissolution kinetics and the weathering of mafic minerals. *Geochim Cosmochim Acta* 43, 717–724. [https://doi.org/10.1016/0016-7037\(79\)90255-2](https://doi.org/10.1016/0016-7037(79)90255-2)
99. Velbel, M.A., 1986. **Influence of surface area, surface characteristics, and solution composition on feldspar weathering rates.** In: J.A. Davis, K.F. Hayes (eds.), *Geochemical Processes at Mineral Surfaces*, American Chemical Society Symposium Series No. 323, pp. 615-634
100. White, A.F., Peterson, M.L., 1990. Chemical Modeling of Aqueous Systems II. *ACS Symp Ser* 461–475. <https://doi.org/10.1021/bk-1990-0416.ch035>
101. Nugent, M.A., Brantley, S.L., Pantano, C.G., Maurice, P.A., 1998. The influence of natural mineral coatings on feldspar weathering. *Nature* 395, 588–591. <https://doi.org/10.1038/26951>
102. White, A.F., Brantley, S.L., 2003. The effect of time on the weathering of silicate minerals: why do weathering rates differ in the laboratory and field? *Chem Geol* 202, 479–506. <https://doi.org/10.1016/j.chemgeo.2003.03.001>
103. Béarat, H., McKelvy, M.J., Chizmeshya, A.V.G., Gormley, D., Nunez, R., Carpenter, R.W., Squires, K., Wolf, G.H., 2006. Carbon Sequestration via Aqueous Olivine Mineral Carbonation: Role of Passivating Layer Formation. *Environ Sci Technol* 40, 4802–4808. <https://doi.org/10.1021/es0523340>

104. Daval, D., Calvaruso, C., Guyot, F., Turpault, M.-P., 2018. Time-dependent feldspar dissolution rates resulting from surface passivation: Experimental evidence and geochemical implications. Earth Planet Sc Lett 498, 226–236. <https://doi.org/10.1016/j.epsl.2018.06.035>
105. Zhu, C., Lu, P., 2009. Alkali feldspar dissolution and secondary mineral precipitation in batch systems: 3. Saturation states of product minerals and reaction paths. Geochim Cosmochim Ac 73, 3171–3200. <https://doi.org/10.1016/j.gca.2009.03.015>
106. Emmanuel, S., Ague, J.J., 2011. Impact of nano-size weathering products on the dissolution rates of primary minerals. Chem Geol 282, 11–18. <https://doi.org/10.1016/j.chemgeo.2011.01.002>
107. White, A.F., Schulz, M.S., Lawrence, C.R., Vivit, D.V., Stonestrom, D.A., 2017. Long-term flow-through column experiments and their relevance to natural granitoid weathering rates. Geochim Cosmochim Ac 202, 190–214. <https://doi.org/10.1016/j.gca.2016.11.042>
108. Brantley, S.L., Shaughnessy, A., Lebedeva, M.I., Balashov, V.N., 2023. How temperature-dependent silicate weathering acts as Earth’s geological thermostat. Science 379, 382–389. <https://doi.org/10.1126/science.add2922>
109. Austin, R., Gatiboni, L., Havlin, J., 2020. Soil Sampling Strategies for Site-Specific Field Management. NC State Extensions, <https://content.ces.ncsu.edu/soil-sampling-strategies-for-site-specific-field-management>
110. Allen, W.J., Sapsford, S.J., Dickie, I.A., 2021. Soil sample pooling generates no consistent inference bias: a meta-analysis of 71 plant–soil feedback experiments. New Phytol 231, 1308–1315. <https://doi.org/10.1111/nph.17455>
111. Carroll, D., 1959. Ion exchange in clays and other minerals. GSA Bulletin 70, 749–779. [https://doi.org/10.1130/0016-7606\(1959\)70\[749:ieicao\]2.0.co;2](https://doi.org/10.1130/0016-7606(1959)70[749:ieicao]2.0.co;2)
112. Sumner, M.E., Miller, W.P., 1996. Cation Exchange Capacity and Exchange Coefficients. In: Sparks, D.L. (ed.), Methods of Soil Analysis Part 3: Chemical Methods, SSSA Book Series 5, Soil Science Society of America, Madison, Wisconsin, 1201-1230.
113. Sparks, D.L., 2003. Environmental soil chemistry (2nd ed.). Academic Press, ISBN 9780126564464, <https://doi.org/10.1016/B978-012656446-4/50006-2>.
114. Kahouli-Brahmi, S., 2008. Technological learning in energy–environment–economy modelling: A survey. Energ Policy 36, 138–162. <https://doi.org/10.1016/j.enpol.2007.09.001>

Supplemental Information

A new soil-based approach for empirical monitoring of enhanced rock weathering rates

Tom Reershemius^{1*} and Mike E. Kelland^{2*}, Isabelle R. Davis^{1,3}, Rocco D'Ascanio¹, Borianna Kalderon Asael¹, Dan Asael¹, Dimitar E. Epihov², David J. Beerling², Christopher T. Reinhard⁴, Noah J. Planavsky¹

¹Department of Earth and Planetary Sciences, Yale University, New Haven, CT, USA

²Leverhulme Centre for Climate Change Mitigation, School of Biosciences, University of Sheffield, Sheffield, UK

³School of Ocean and Earth Science, University of Southampton Waterfront Campus, Southampton, UK

⁴School of Earth and Atmospheric Sciences, Georgia Institute of Technology, GA, USA

*corresponding and equal contribution authors: tom.reershemius@yale.edu, mekelland1@sheffield.ac.uk

1 Supplemental Materials and Methods

1.1 Mesocosm design and construction

Replicated mesocosms (**Supplemental Figure S1a**) ($n = 7$) for the four soil treatments in this study (NPK –basalt, NPK +basalt, manure –basalt, manure +basalt) were constructed from two sections of polyvinyl chloride (PVC) pipe, joined by a pair of PVC endcaps fixed in a back-to-back arrangement (152 mm internal diameter pipe, 160 mm internal diameter endcaps; Brett Martin, Newtownabbey, UK). The freestanding mesocosms were stabilised with a 170 mm × 190 mm acrylic baseplate fixed to a further 160 mm internal diameter endcap that was attached to the lower pipe section. Weight-bearing external joints were secured with PVC weld cement (Tangit ABS; Henkel, Düsseldorf, Germany) and internal seals were formed from high-strength polyurethane sealant (PU18; Bond It Ltd, Elland, UK).

Substrate was loaded into the 600 mm long top section and leachate collection apparatus were housed in the 400 mm long lower section. The joint attaching these pipe sections was fitted with a 20 mm internal diameter nylon nozzle to direct leachate into a high-density polyethylene bottle via a polypropylene funnel (1 L narrow-neck polyethylene bottle, 150 mm lightweight polypropylene filter funnel; Azlon, Stoke-on-Trent, UK). Soil particle migration into the leachate nozzle was reduced by emplacing a 60 mm deep drainage layer in the base of the substrate-holding top section, comprised of 20 mm diameter polyoxymethylene balls (Bearing Warehouse Ltd, Sheffield, UK). A detachable 3-ply opaque mylar membrane (Reflex Total Blackout; GroWell Horticulture Ltd, Sheffield, UK) was used to reduce algal growth in the leachate collection apparatus.

1.2 Substrate preparation and characterization

Mildly acidic (pH 6.45) agricultural soil of clay-loam texture (29.0, 34.3 and 36.7% by mass of clay (<2 µm), silt (2-60 µm) and sand (60-2,000 µm), respectively) was collected from farmland under *Brassica napus* (oil seed rape) cultivation at the Game and Wildlife Conservation Trust, Allerton Project, Leicestershire, UK (latitude 52.611286 °N, longitude 0.831559 °W). The soil had

an initial cation exchange capacity of 22.0 cmol (p⁺) kg⁻¹, with a base saturation of 70.0%, calcium saturation of 63.4%, and a gravimetric water content (GWC) at field capacity of 0.68 g g⁻¹. The soil total carbon concentration was 2.3 wt% and the soil organic carbon concentration was 1.1 wt%.

Collected soil was manually comminuted at 18°C and stored in partially sealed polypropylene bags to reduce moisture loss. Large stones and invertebrates were removed before the soil was passed through a woven stainless-steel sieve (2 mm mesh size; Fisher Scientific UK Ltd, Loughborough, UK). After comminution, the soil had a GWC of 0.28 g g⁻¹. Organic fertilizer for the experiment was derived from cow manure collected from Hope Farm, Hassop, UK. The manure was air dried for 30 days, then manually comminuted at 18 °C and passed through a 2 mm mesh size stainless-steel sieve.

Mesocosms were filled with substrate in a sub- and top-soil arrangement to simulate a tillage regime (3:1 mass ratio of sub- to top-soil) (**Supplemental Figure S1b**). The total dry mass of soil in each mesocosm was 8.252 kg, which – being compacted to a column height of 500 mm – had an average bulk density of 0.91 kg L⁻¹. Basalt and fertilizer were added, as required, to the topsoil only and were mixed thoroughly into the substrate immediately prior to mesocosm filling on day 0. A total mass of 91 g (equivalent to 5.0 kg m⁻²) of basalt (see below) was added to treated mesocosms. Soils treated with chemical fertilizer received individually weighed quantities of analytical-grade compounds (0.347 g of urea, 1.633 g of powdered diammonium phosphate and 1.482 g of powdered potassium chloride), which were estimated to compensate for soil nutrient losses to the crop and leachate during the experiment. Mesocosms treated with organic fertilizer received 17.7 g (equivalent to 1.0 kg m⁻²) of air-dried cow manure, which contained 2.57, 1.23 and 3.08% total nitrogen, phosphorus pentoxide and potassium oxide, respectively. The manure application rate was calculated to approximately equal the total nitrogen application rate in the chemical fertilizer treatment, being 25 g N m⁻² (250 kg N ha⁻¹).

Initial soil pH was measured using a Jenway 3540 Bench Combined Conductivity/pH Meter (Jenway, Stone, UK) calibrated with standard solutions at pH 4, 7 and 14. Prior to pH determination, 15 g of air-dried soil was thoroughly mixed with 30 ml of deionized water in a 100 ml borosilicate glass beaker using a glass stirrer. The solution was then left for 30 minutes before recording the pH of the slurry to 0.01 pH units. Soil carbon measurements were made using a Vario EL Cube Carbon-Nitrogen Analyzer (Elementar, Stockport, UK), with soil organic carbon content determined by comparing carbon concentrations before and after soil treatment with 6 M HCl (soil:acid ratio of 90 mg to 0.5 mL).

1.3 Basaltic rock preparation and characterization

Crushed basalt of middle Miocene age and belonging to the ‘Prineville Chemical Type Unit’ of the Columbia River Basalt was sourced from the Cascade Range, Oregon (Central Oregon Basalt Products LLC, Madras, ORE, USA). The basalt was passed through a series of stainless-steel sieves of decreasing mesh size (250 µm, 100 µm and 50 µm mesh size), suspended in analytical-grade ethanol and sonicated for 30 minutes in a 5 L Pyrex beaker to separate submicron particles from larger grains. The suspension was then left for 24 h (sufficient to settle particles with diameters > 1 µm) after which the supernatant was decanted and the settled basalt material was

exposed to the air for 72 h to evaporate the residual ethanol. The particle size distribution of the treated basalt was measured using an LA-950 laser diffraction particle size distribution analyzer (Horiba UK Ltd, Northampton, UK), where the particle diameter range was found to be 1.5-300 μm and the P80 value (the size at which 80% of the particles have diameters less than or equal to) was 35 μm (**Supplemental Figure S2**). Specific surface area of the treated basalt was determined using an Anton Paar Nova 800 Brunauer Emmett Tell (BET) surface area analyzer in the Yale Geochemistry Center and found to be 10.22 $\text{m}^2 \text{g}^{-1}$. Error was estimated to be 0.01 $\text{m}^2 \text{g}^{-1}$, based on a 5-point analysis.

The mineralogy of the basalt (**Supplemental Figure S3**) was determined using X-ray diffraction (XRD) analysis at the British Geological Survey (BGS) Keyworth laboratories, following the protocol reported in Lewis et al. (2021). The carbon dioxide removal potential of the basalt feedstock, E_{pot} (i.e. the maximum amount of carbon dioxide consumed if all basalt were to react with proton equivalents from carbonic acid), can be quantified using a modified Steinour formulation, which relates maximum theoretical carbon dioxide reaction with elemental composition of silicate feedstocks (Steinour, 1959; see e.g., Fernández Bertos et al., 2004; Gunning et al., 2010; Renforth, 2019; Bullock et al., 2021). The Steinour formulation using major cations for alkaline minerals is given as:

$$E_{pot} = \frac{\eta M_{CO_2}}{100} * \left(\frac{\alpha \text{CaO}}{M_{CaO}} + \frac{\beta \text{MgO}}{M_{MgO}} + \frac{\varepsilon \text{Na}_2\text{O}}{M_{Na_2O}} + \frac{\theta \text{K}_2\text{O}}{M_{K_2O}} \right)$$

where M_i is molar mass; η , α , β , ε , and θ are stoichiometric constants (in this case with values 2.0, 1.0, 1.0, 1.0, and 1.0 respectively); and CaO, MgO, Na₂O and K₂O are abundances of major oxides in the feedstock. Using this formulation, with the values for major oxide abundance given in **Supplemental Table T1**, E_{pot} for the basalt feedstock used here is 211.81 $\text{kgCO}_2 \text{t}^{-1}$. This assessment is a conservative estimate representing incongruent dissolution (i.e., does not include cations that will react to form secondary minerals, including Al³⁺ and Fe²⁺; e.g., Rinder and von Hagke, 2021). Note that some previous authors have simplified this formulation to only include CaO and MgO, when assessing E_{pot} for fast-weathering Ca- and Mg-silicates (e.g., Renforth, 2012), which are the most abundant cations. In this study, we ignore the contribution of K⁺ to carbon dioxide removal, due to its presence in NPK fertilizers; as such, when excluding K₂O, E_{pot} for the basalt feedstock is revised to 183.56 $\text{kgCO}_2 \text{t}^{-1}$.

1.4 Plant varieties and growth conditions

A single specimen of dwarf hybrid *Sorghum bicolor* (Pennsylvania 115, Oakbank Game and Conservation, Cambridgeshire, UK) was cultivated in each mesocosm. Approximately 600 seeds were germinated on filter paper (Whatman #1; Cytiva, Sheffield, UK) moistened with distilled water, placed in grip seal polyethylene bags and incubated at 25°C in darkness for 24 h. 144 seeds of similar radicle length (ca. 5 mm) were selected for planting in 24-cell seed trays containing soil from the same field site. Seed trays were transferred to a growth room and maintained at 60–70% relative humidity, with an 18 h day length and 25/17°C day/night temperatures. After 24 h, 87 seedlings emerged from the soil, of which the 28 largest were grown for a further 9 d and chosen at random for transplantation to mesocosms on day 0.

Additive CO₂ was used to sustain atmospheric concentrations of 400 ppm in the controlled environment and a photosynthetic photon flux density of 800 $\mu\text{mol photons m}^{-2} \text{s}^{-1}$ was maintained throughout the 18 h days between emergence and boot stage (days 0-60). From day 61 onwards the day length was reduced to 10 h and on day 115 (at physiological maturity) *Sorghum* seeds and shoots were harvested. Henceforth a fallow period was simulated by reducing the day/night temperatures to 5/3°C and maintaining relative humidity at 75% until the experiment was terminated on day 235.

1.5 Irrigation regime

Throughout the *Sorghum* lifecycle, mesocosms were weighed every 3 days using a portable laboratory balance (Navigator NVT; Ohaus, Parsippany, NJ, USA) to estimate depth-averaged soil GWC. An artificial rainwater solution (**Supplemental Table T2**) was then used to approximately compensate for soil water losses via evapotranspiration, with equal volumes of solution being supplied to each mesocosm (**Supplemental Figure S4**). Irrigation water was delivered manually to the top surface of each soil column using a 1.5 L low-pressure portable sprayer (Exo Terra, Castleford, UK), with amounts measured gravimetrically to the nearest gram. Approximately every 12 d between day 0 and day 81, equal volumes of additional irrigation solution were supplied to all soil columns to produce leachate for geochemical analysis. During the simulated fallow period (days 115-235) mesocosms were weighed every 14 d and variably irrigated to maintain soil GWC at 0.38 g g⁻¹.

1.6 Soil sample preparation and analysis

Soil samples were collected from all mesocosms after 235 days. Substrate was excavated from the mesocosms in five separate layers: the topsoil/amended layer (0-120 mm depth), three intermediate subsoil layers (120-240, 240-360, 360-480 mm depth) and the bottommost subsoil layer (480-500 mm depth). Each soil layer was manually comminuted into a bulk sample, homogenized, air dried at 60 °C for 48 h, and passed through a 2mm steel sieve. 100 mg of dried sample was subjected to leaching with a 1N ammonium acetate solution at pH = 8.2 in order to remove the exchangeable fraction from the solid phase (after Chapman, 1965). The resultant solid sample was dried at 60°C overnight, then heated at 600 °C for 24 hours to remove organic matter in the soil mixture. The ashed sample was then dissolved in a mixture of aqua regia (hydrochloric and nitric acid) and hydrofluoric acid as follows: 10ml aqua regia was added to Teflon beakers containing ashed sample, left to sit for 4 hours after which 1ml hydrofluoric acid was added, the beakers capped and left on a hotplate for 24 hours at 100°C. Samples were then uncapped and left to dry down on a hotplate at 90°C. Samples were raised in nitric acid and diluted to run on a Thermo Scientific iCAP Triple Quadrupole inductively coupled plasma mass spectrometer (ICP-MS) at the Yale Geochemistry Center. In order to reduce analytical error, we measured the concentrations of key elements (Ca, Mg, Ti) using an isotope dilution method (see Section 6.7).

1.7 Analytical requirements: isotope dilution inductively coupled plasma mass spectrometry (ID-ICP-MS)

). In order to reduce analytical error we measure the concentrations of key elements (Ca, Mg, Ti) using an isotope dilution method. The amount of an element in the sample, n_{sam} , is given by:

$$n_{sam} = n_{spk} \frac{R_{spk} - R_{mix} \sum_i R_{isam}}{R_{mix} - R_{sam} \sum_i R_{ispk}}$$

where R is the ratio of two isotopes, and $\sum_i R_i$ is the sum of ratios of all isotopes to a reference isotope (e.g., Inghram, 1954; see also Evans and Clough, 2005; Stracke et al., 2014). We use an isotope spike ‘cocktail’, doped with isotopes of Mg, Ti, and Ca found in lower abundance in natural samples (**Supplemental Figure S5**). Isotope spikes are prepared from powders of spiked TiO₂, MgCO₂ and CaCO₂. The pure spike Mg and Ca carbonate powders are digested using HCl, and the Ti oxide using HNO₃+HCl+HF. Following the digest each spike solution is calibrated by measuring the relative concentration of Mg, Ca, and Ti isotopes on a ThermoFisher Neptune Plus multicollector ICP-MS for ~48 hours. Estimate of the error on the spike determination are < 0.1 ‰ based on replicate analysis. Individual spike solutions are then used to make an isotope spike ‘cocktail’ solution containing Mg, Ca and Ti spikes. The cocktail is added to each sample during the dissolution stage of sample preparation to ensure sample-spike equilibration.

Isotope dilution allows for sample-specific calculation of element concentrations, unlike a calibration curve method whereby standards of known concentration are run to relate element intensities (in counts per second) to concentration. Isotope dilution therefore corrects for matrix effects, mass bias, and instrument drift, and thus improves both accuracy and precision of measured concentrations (**Figure 3**; see also Willbold and Jochum, 2005). In addition to an iCAP TQ ICP-MS, we ran standards on a other ICP-MS models in order to test the data quality achieved by a variety of widely available instruments (a Perkin Elmer NexION 5000 Multi-Quadropole ICP-MS and a Thermo Scientific Element High Resolution Magnetic Sector ICP-MS).

1.8 Leachate, soil extract and plant sample preparation and analysis

Leachate was prepared for cation analysis by filtration of subsamples through a 0.45 µm cellulose nitrate filter (Minisart: Sartorius, Goettingen, Germany) and stabilization in a matrix of 2% (vol%) analytical-grade nitric acid. Harvested *Sorghum* root, shoot and seed tissues were dried in a forced-air oven at 60 °C for 48 h and comminuted separately using a laboratory grinding mill (Model: A10 S2, IKA-Werke GmbH & CO. KG, Staufen, Germany). Oven-dried, powdered tissue samples were then subjected to a 45-min microwave-assisted (Model: Multiwave; Anton Paar Ltd, St Albans, UK) nitric acid-hydrogen peroxide digest (0.2 g tissue:3 mL nitric acid:3 mL MQ water:2ml hydrogen peroxide), after which extracts were prepared for cation analysis by centrifugation and filtration of the supernatant through a 0.45 µm filter. Multi-element cation analysis of all prepared leachate, plant and soil extracts was conducted at the School of Biosciences, University of Nottingham (Sutton Bonington Campus) using an iCAP Q ICP-MS (Thermo Fisher Scientific, Bremen, Germany).

1.9 Cases signifying breakdown of the TiCAT scheme

Several cases signify a breakdown in the simple mixing scheme used for TiCAT (**Supplemental Figure S6**):

1. $\Delta CAT < 0$ suggests that precipitation of a secondary mineral phase or phases containing cations has occurred between application of basalt and post-application sampling. This is pertinent to calculating initial CDR rates, as CO₂ is released by these reactions (with the exception of salt formation) (**Supplemental Figure S6a**).

2. $Ti_{end} < Ti_{soil}$ indicates that the soil baseline used is unsuitable, assuming no mass transport has occurred, and as such a more suitable soil baseline is required to obtain a reliable estimate of feedstock dissolution (**Supplemental Figure S6b**).
3. $CAT_{end} < CAT_{soil}$ indicates dissolution and loss of cations from the background soil. In this case it is necessary to apply the limit $-ΔCAT = CAT_{add}$ (i.e., $f_{dissolution} = 1$) (**Supplemental Figure S6c**).

In our experimental method we remove the exchangeable fraction (non-mineral-bound cations occupying exchange sites on clay mineral surfaces). However, clay and carbonate minerals are included in the solid phase of digested soil samples, which could result in an underestimate of the extent of silicate mineral dissolution given that secondary mineral formation could reincorporate mobile cations into the solid phase following dissolution. As a result, our technique should be considered to track net cation mobility from the system, including the impact of secondary phase formation.

1.10 Calculating an initial CDR rate using TiCAT

The TiCAT approach provides a time-integrated estimate of the amount of feedstock that has dissolved between application and post-application sampling. This can be directly converted into an initial CDR rate by using a modified Steiour formulation (*Supplemental Information Section 1.3*). Assuming $f_{dissolution}$ for relevant cations CAT (Na^+ , Ca^{2+} , Mg^{2+}) in each sample (see **Figure S7**) is representative of $f_{dissolution}$ for each mesocosm, we can calculate the total mass of each cation mobilized from applied feedstock over a given area:

$$f_{dissolution} * A_{CAT} (kg m^{-2}) = A_{CATdiss} (kg m^{-2}) ,$$

where A_{CAT} is the application rate of the cation CAT, calculated as:

$$A_{basalt} (kg m^{-2}) * wt\%[CAT] = A_{CAT} (kg m^{-2}) .$$

We then convert $A_{CATdiss}$ to an amount (in mol m^{-2}) and apply the relevant Steiour coefficient to convert from mol(CAT) to mol(CO₂) consumed. Converting to a mass in kg m^{-2} gives the total potential CO₂ removed by weathering of the feedstock for each cation; summed, these give total CO₂ removed by weathering of the feedstock in kg m^{-2} .

Here, we use as our c_{soil} endmember the mean concentration of cations obtained from the bottommost subsoil layer (480-500mm). This is more representative of an untreated soil within our mesocosms than using a single sample of bulk soil taken before the experiment was started (see **Supplemental Figures S8 and S9**). The total amount of metal cations added to each mesocosm via irrigation was negligible (see **Supplemental Figure S4 and Supplemental Table ST2**).

Supplemental Tables

Table ST1. Chemical composition (major oxides) of basalt feedstock used, Columbia River Basalt, Prineville Chemical Type Unit. Bulk rock total digest (HF+HNO₃+HCl), measured on Element HR-ICP-MS. See also Kelland et al., 2020, and Lewis et al., 2021, for further chemical and textural information about the feedstock used.

Oxide	Concentration (wt%)
CaO	5.26
MgO	2.37
Na₂O	3.79
K₂O	3.02

Table ST2. Chemical composition of artificial rainwater irrigation solution.

Salt	Solution concentration (mg L⁻¹)
NaNO₃	0.000135
NaCl	0.004790
CaCl₂·2H₂O	0.001100
K₂SO₄	0.000450
MgSO₄·7H₂O	0.002050
(NH₄)₂SO₄	0.002270

Supplemental Figures

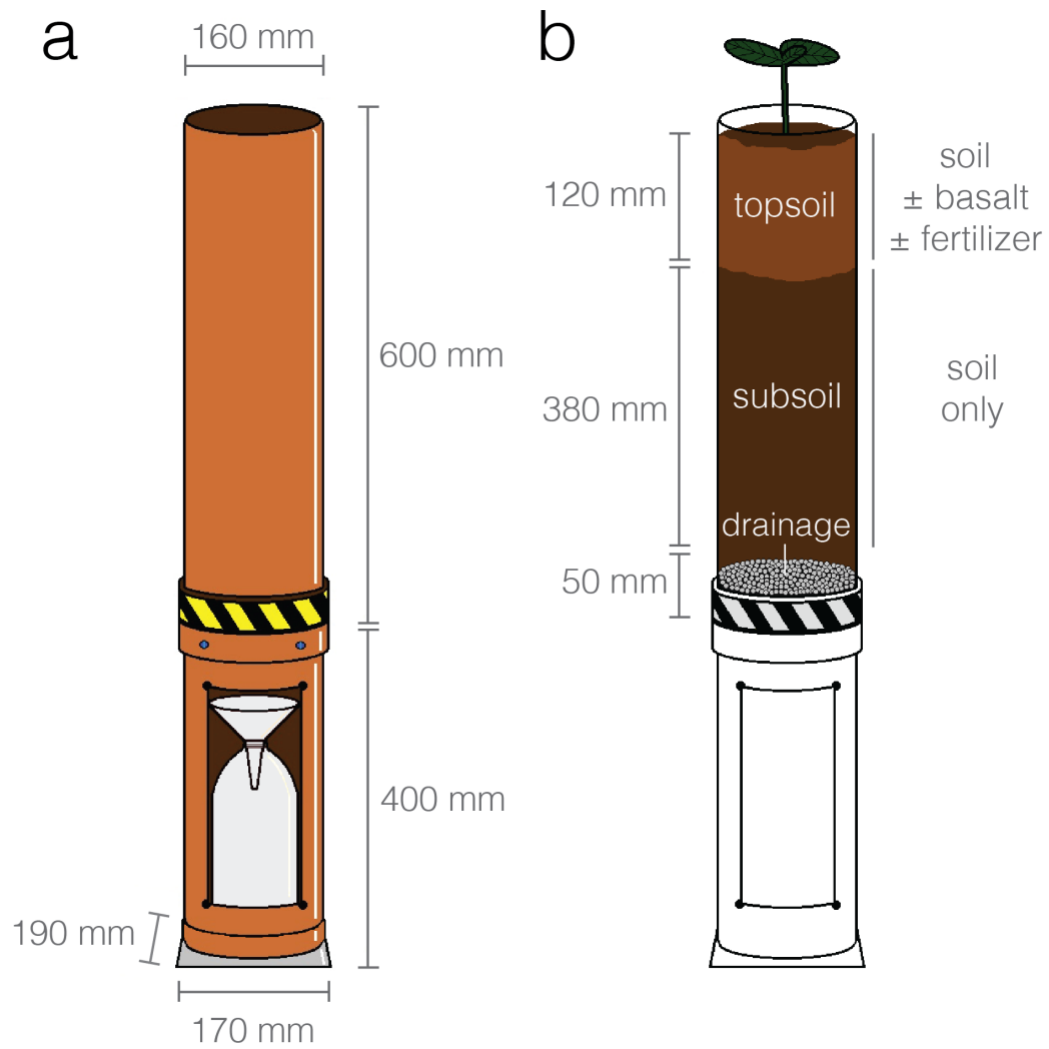


Figure S1. Mesocosm design. (a) Schematic of mesocosm exterior; and (b) cutaway indicating sub- and top-soil arrangement simulating tillage regime.

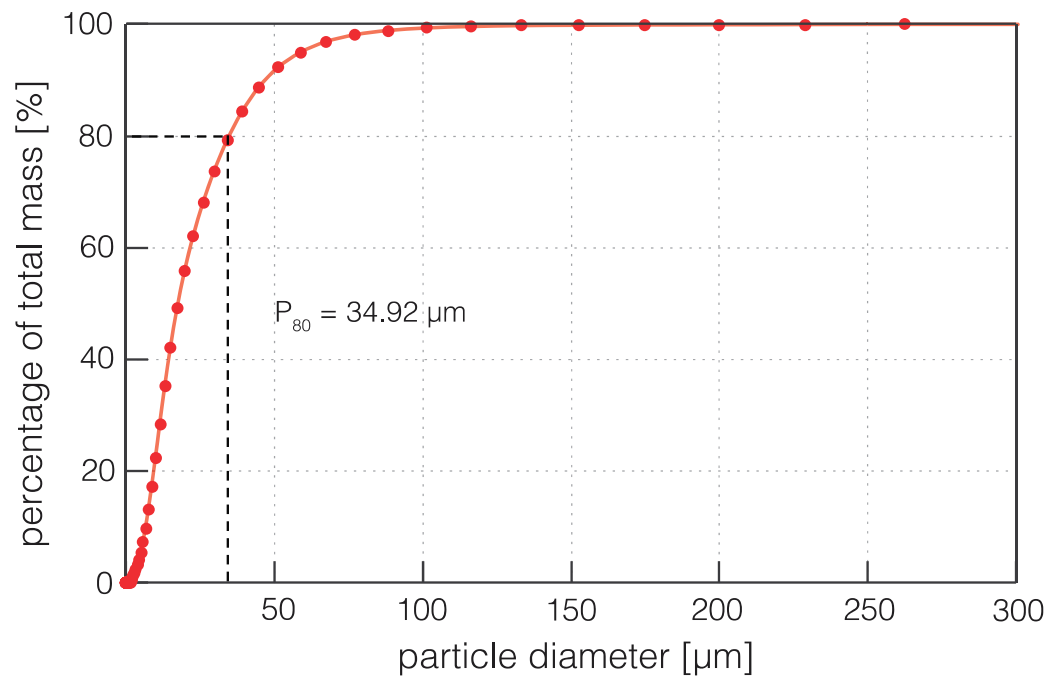


Figure S2. Cumulative particle size distribution of basalt material. Determined by laser diffraction particle size distribution analysis.

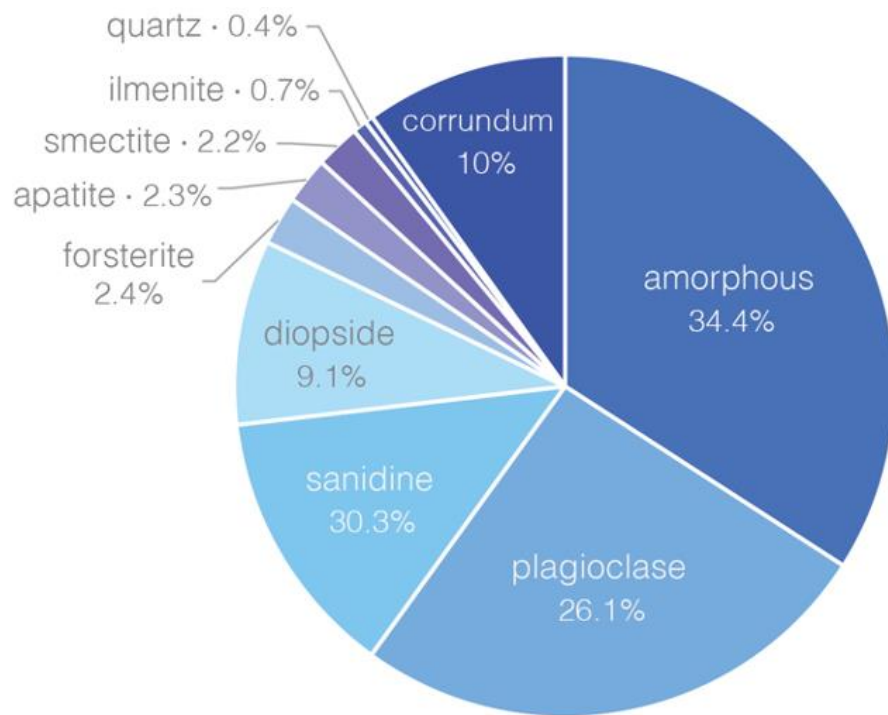


Figure S3. Mineralogy of basalt material. Determined by X-Ray Diffraction analysis.

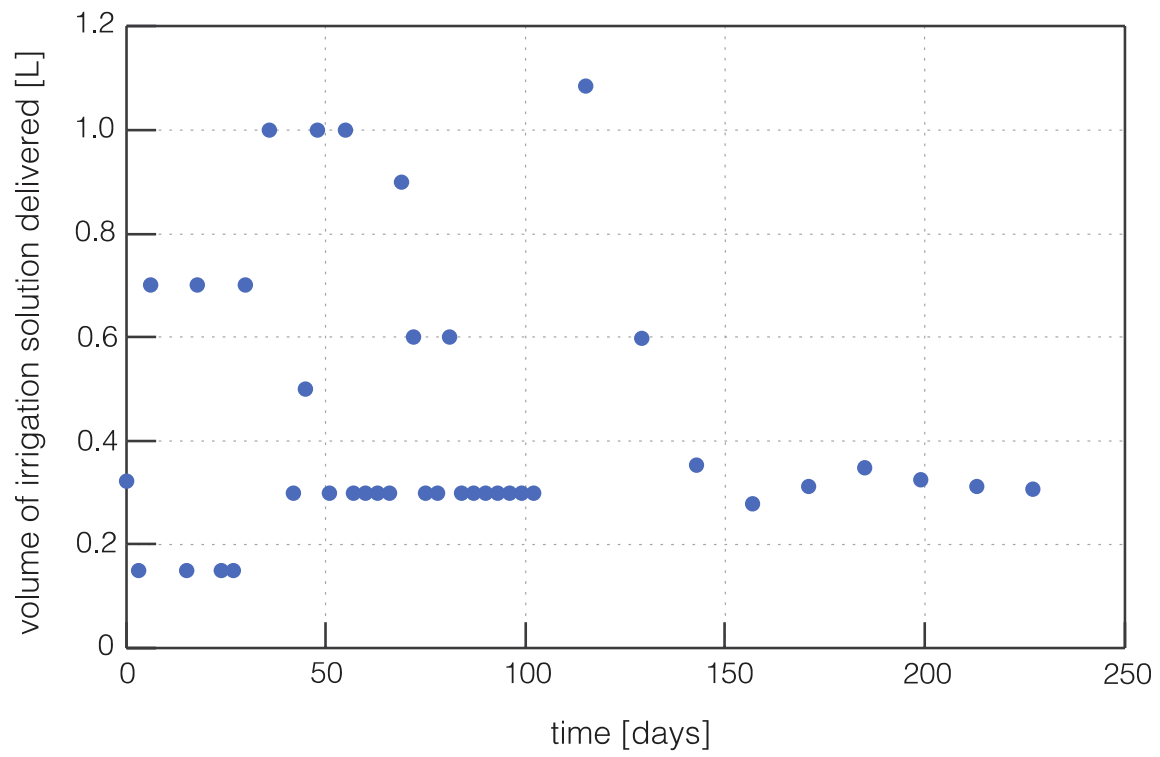


Figure S4. Irrigation schedule. Volume of irrigation solution added to mesocosms.

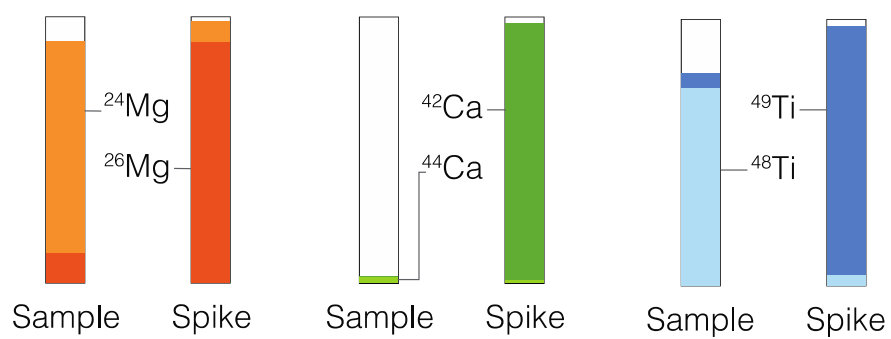


Figure S5. Isotopic composition of key elements for which isotope dilution was used to reduce analytical error in this study, in natural samples (left) and the isotope spike cocktail added to the samples (right). Isotopes shown are those used in calculations.

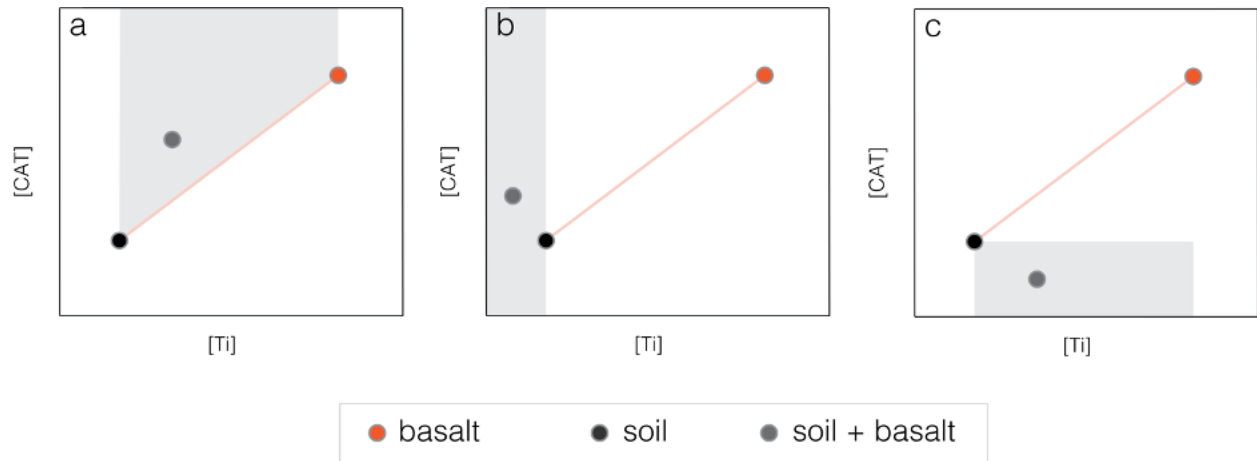


Figure S6. Cases where the composition of soil+basalt mixtures fall outside of the TiCAT framework: $\Delta\text{CAT} < 0$, indicating precipitation of CAT into a secondary mineral phase (a); $\text{Ti}_{\text{end}} < \text{Ti}_{\text{soil}}$, indicating the soil baseline value for Ti is not suitable (b); $\text{CAT}_{\text{end}} < \text{CAT}_{\text{soil}}$, indicating dissolution of CAT from soil (c).

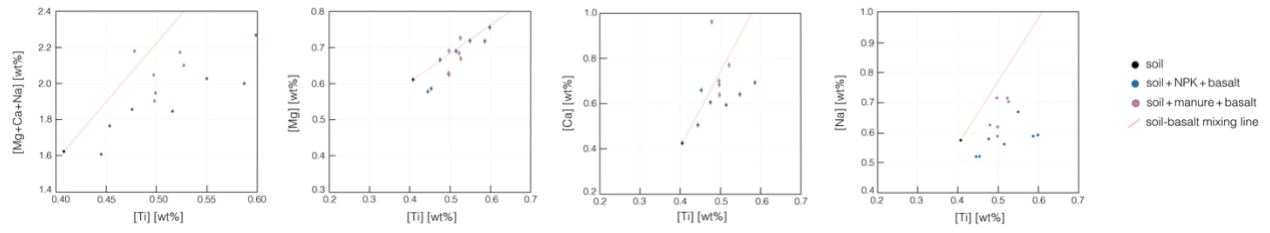


Figure S7. Concentration in ashed solid samples of Mg, Ca, and Na from the “topsoil” depth interval (0-12 cm) in all mesocosms in this study. “Soil” indicates the the mean concentration of cations obtained from the bottommost subsoil layer (480-500mm). Analytical error is shown (note the error bar for Na is smaller than the symbol).

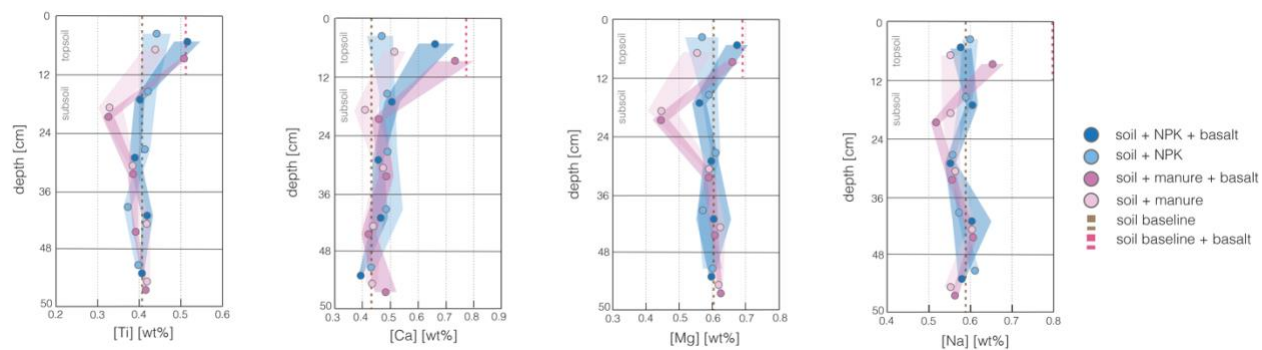


Figure S8. Depth profiles of concentration in ashed solid samples of Ti, Ca, Mg, and Na from mesocosms in this study. Points are averages of all columns for the relevant treatment, and shaded envelopes show σ . Samples are all homogenized across the depth interval between solid horizontal bars. Dashed brown vertical line indicates the composition of the baseline soil endmember. Dashed red vertical line indicates the composition of a fully homogenized baseline soil + basalt mixture in the topsoil layer, where the average additional amount of Ti is used to calculate average basalt addition rate in samples.

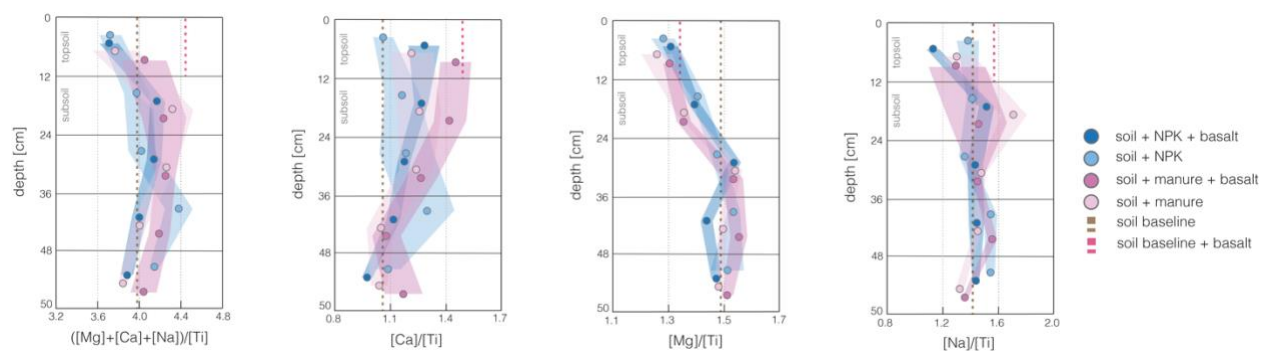


Figure S9. Depth profiles of ratios in concentration in ashed solid samples of $(\text{Ca}+\text{Mg}+\text{Na})/\text{Ti}$, Ca/Ti , Mg/Ti , and Na/Ti from mesocosms in this study. Points are averages of all columns for the relevant treatment, and shaded envelopes show 2σ . Samples are all homogenized across the depth interval between solid horizontal bars. Dashed brown vertical line indicates the composition of the baseline soil endmember. Dashed red vertical line indicates the composition of a fully homogenized baseline soil + basalt mixture in the topsoil layer, where the average additional amount of Ti is used to calculate average basalt addition rate in samples.

References

- Andersen, J.E.T., 2014. On the development of quality assurance. *Trac Trends Anal Chem* 60, 16–24. <https://doi.org/10.1016/j.trac.2014.04.016>
- Chapman, H.D. 1965. Cation-exchange capacity. In: C.A. Black (ed.). *Methods of soil analysis - Chemical and microbiological properties*. *Agronomy* 9:891-901.
- Eggen, O.A., Reimann, C., Flem, B., 2019. Reliability of geochemical analyses: Deja vu all over again. *Sci Total Environ* 670, 138–148. <https://doi.org/10.1016/j.scitotenv.2019.03.185>
- Evans, E.H., Clough, R., 2005. Isotope dilution analysis. In: Worsfold, P., Townshend, A., Poole, C. (eds.). *Encyclopedia of Analytical Science* (2nd ed.). Elsevier, 545-553. <https://doi.org/10.1016/B0-12-369397-7/00301-0>
- Fernández Bertos, M., Simons, S.J.R., Hills, C.D., Carey, P.J., 2004. A review of accelerated carbonation technology in the treatment of cement-based materials and sequestration of CO₂. *J Hazard Mater* 112, 193–205. <https://doi.org/10.1016/j.jhazmat.2004.04.019>
- Gunning, P.J., Hills, C.D., Carey, P.J., 2010. Accelerated carbonation treatment of industrial wastes. *Waste Manage* 30, 1081–1090. <https://doi.org/10.1016/j.wasman.2010.01.005>
- Inghram, M.G., 1954. Stable isotope dilution as an analytical tool. *Ann Rev Nucl Sci* 4:1, 81-92. <https://doi.org/10.1146/annurev.ns.04.120154.000501>
- Lewis, A.L., Sarkar, B., Wade, P., Kemp, S.J., Hodson, M.E., Taylor, L.L., Yeong, K.L., Davies, K., Nelson, P.N., Bird, M.I., Kantola, I.B., Masters, M.D., DeLucia, E., Leake, J.R., Banwart, S.A., Beerling, D.J., 2021. Effects of mineralogy, chemistry and physical properties of basalts on carbon capture potential and plant-nutrient element release via enhanced weathering. *Appl Geochem* 132, 105023. <https://doi.org/10.1016/j.apgeochem.2021.105023>
- Renforth, P., 2012. The potential of enhanced weathering in the UK. *Int J Greenh Gas Con* 10, 229–243. <https://doi.org/10.1016/j.ijggc.2012.06.011>
- Renforth, P., 2019. The negative emission potential of alkaline materials. *Nat Commun* 10, 1401. <https://doi.org/10.1038/s41467-019-09475-5>
- Rinder, T., von Hagke, C., 2021. The influence of particle size on the potential of enhanced basalt weathering for carbon dioxide removal - Insights from a regional assessment. *J Clean Prod* 315, 128178. <https://doi.org/10.1016/j.jclepro.2021.128178>
- Steinour, H.H., 1959. Some effects of carbon dioxide on mortars and concrete-discussion, *J. Am. Concrete I* 30, 905.

Stracke, A., Scherer, E.E., Reynolds, B.C., 2014. Application of isotope dilution in geochemistry. *Treatise on Geochemistry* (Second Edition) 71–86. <https://doi.org/10.1016/b978-0-08-095975-7.01404-2>

Willbold, M., Jochum, K.P., 2005. Multi-Element Isotope Dilution Sector Field ICP-MS: A Precise Technique for the Analysis of Geological Materials and its Application to Geological Reference Materials. *Geostand Geoanal Res* 29, 63–82. <https://doi.org/10.1111/j.1751-908x.2005.tb00656.x>